J|A|C|S
ARTICLES
Published on Web 11/08/2006

Distinct Kinetic Pathways Generate Organogel Networks with Contrasting Fractality and Thixotropic Properties

Xiao Huang,[†] Srinivasa R. Raghavan,[‡] Pierre Terech,[§] and Richard G. Weiss*,[†]

Contribution from the Department of Chemistry, Georgetown University, 37th and O Streets, NW, Washington, DC 20057-1227, Department of Chemical and Biomolecular Engineering, University of Maryland, College Park, Maryland 20742-2111, and CEA-Grenoble, DRFMC/SI3M Laboratoire Physico-Chimie Moleculaire 17, Rue des Martyrs 38054 Grenoble cedex 9, France

Received August 11, 2006; E-mail: weissr@georgetown.edu

Abstract: The kinetics of the isothermal transformation of sols, comprised of a low molecular-mass organogelator (LMOG) and an organic liquid, to their organogel phases have been followed by circular dichroism (CD), fluorescence, small angle neutron scattering (SANS), and rheological methods. The thixotropic properties (in the sense that severe shearing followed by rest lead to reestablishment of viscoelasticity) of the gels have been examined as well by rheological measurements. The compositions of the samples were either 5α-cholestan-3β-yl *N*-(2-naphthyl) carbamate (**CNC**) in an *n*-alkane (*n*-octane or *n*-dodecane) or 3β-cholesteryl *N*-(2-naphthyl) carbamate (**CeNC**) in ethyl acetate. Values of D_f, the mass fractal dimension of the microcrystalline self-assembled fibrillar networks (SAFINs) in the gels, have been extracted from the kinetic data using a model developed by Dickinson (*J. Chem. Soc., Faraday Trans.* **1997**, *93*, 111). The D_f values, 1.1−1.3 for the **CeNC** gels and 1.3−1.4 or 1.6−1.8 (depending on the temperature of incubation of the sol phase) for **CNC** gels, are consistent with the gel network structures observed by optical microscopy. In addition, comparison of the temperature dependence of both *n* (the Avrami component) and *K* (the Avrami "rate constant") for **CeNC**/ethyl acetate gelation with those reported previously for gelation of **CNC**/*n*-alkane sols demonstrate that the very small change of a single bond in **CNC** to a double bond in **CeNC** causes significant differences in their gelation abilities and gel properties. The rheological measurements on **CNC**/*n*-alkane gels with spherulitic SAFIN units, formed by incubation of their sols at ≤28 °C, indicate that they are thixotropic. Gels with the same chemical composition but formed by incubation of their sols at ≥30 °C, leading to fiberlike SAFIN units, remain liquidlike after shearing regardless of the periods they are at rest. The time-dependent viscoelastic properties of the gel networks are treated according to a stretched exponential model. The observations from these studies provide detailed insights into the mechanisms of formation of molecular organogel phases and demonstrate the extreme sensitivity of the SAFINs and viscoelastic properties of such organogels to slight modifications in LMOG structure or sample history.

Introduction

Molecular organogels, a type of soft matter,[1] have experienced an enormous increase in interest during the past decade. They consist of a low concentration (usually ≤2 wt %) of a low-molecular-mass molecule (LMOG) and a liquid.[2] The self-assembled fibrillar networks (SAFINs) of most molecular organogels are formed thermoreversibly by cooling a solution or sol and are dissolved by heating the gel above a transition temperature (T_g).[2] Although fractal structures of polymer gels are more common and have been studied experimentally, theoretically, and by computer simulation for many years,[3,4] some SAFINs of LMOG gels are also fractal[5] and others are thixotropic (i.e., with time, they slowly recover their elasticity after experiencing intense shear).[6]

[†] Georgetown University.
[‡] University of Maryland.
[§] CEA-Grenoble.

(1) Jones, R. A. L. *Soft Condensed Matter*; Oxford University Press: Clarendon, 2002.
(2) (a) Terech, P.; Weiss, R. G. *Chem. Rev.* **1997**, *97*, 3133−3159. (b) Abdallah, D. J.; Weiss, R. G. *Adv. Mater.* **2000,** *12*, 1237−1247. (c) Weiss, R. G.; Terech, P., Eds. *Molecular Gels. Materials with Self-Assembled Fibrillar Networks*; Springer: Dordrecht, 2006. (d) George, M; Weiss, R. G. *Acc. Chem. Res.* **2006**, *39*, 489−497.
(3) (a) Nakayama, T.; Yakubo, K. *Fractal Concepts in Condensed Matter Physics*; Springer: Berlin, 2003. (b) Rothschild, W. G. *Fractals in Chemistry*; John Wiley & Sons: New York, 1998. (c) Deway, T. G. *Fractals in Molecular Biophysics*; Oxford University Press: New York, 1997.
(4) For some pertinent references, see: (a) de Gennes, P. G. *Scaling Concepts in Polymer Physics*; Cornell University Press: Ithaca, NY, 1979. (b) Stauffer, D.; Coniglio, A.; Adam, M. *Adv. Polym. Sci.* **1979**, *44*, 103−158. (c) Hendricks, E.; Ernst, M.; Ziff, R. *J. Stat. Phys.* **1983**, *31*, 519−563. (d) Meakin, P. *Phys. Rev. Lett* **1983**, *51*, 1119−1122. (e) Kolb, M.; Botet, R.; Jullien, R. *Phys. Rev. Lett.* **1983**, *51*, 1123−1126. (f) Jullien, R.; Hasmy, A. *Phys. Rev. Lett.* **1995**, *74*, 4003−4006. (g) Coniglio, A.; Stanley, H. E.; Klein, W. *Phys. Rev. B* **1982**, *25*, 6805−6821. (h) Tanaka, F.; Matsuyama, A. *Phys. Rev. Lett.* **1989**, *62*, 2759−2762.

10.1021/ja0657206 CCC: $33.50

One of the most important defining parameters of a fractal object is its mass fractal dimension, D_f.[3] Several techniques have been developed to measure the D_f of gel-like materials. They include rheological measurements,[5a,b,7] light, neutron, and X-ray scattering methods,[3b,8] and adsorption−desorption experiments.[9] A real-space method, fractal analysis of digitized gel images, has been used recently[3,b10] to correlate measured variables and values of D_f based on physical models intended for application to polymer gels or porous materials such as zeolites.[3,a,11] Although those studies have yielded very useful information, the models employed may not be applicable directly to molecular organogels; the construction of three-dimensional SAFINs from polymer gellants begins with at least one dimension of the networks (N.B., the polymer chains) already in place, whereas those from LMOGs start with "zero" dimensional building blocks.[2d]

A fractal dimension provides direct information about the structures of gels but indirect information, if any, about the kinetics of their formation.[3] In principle, fractal dimensions should be obtainable from the kinetics of gelation, and they have been in a different context to describe self-similarities in the aggregation of some colloidal gels.[12] In that regard, Liu and co-workers[5c,d] have studied the formation of organogels comprised of *N*-lauroyl-L-glutamic acid di-*n*-butylamide as the LMOG and *iso*-stearyl alcohol as the liquid using the Avrami equations,[13] and they have correlated the so-called Avrami component *n*, which is related to the dimensionality of crystal growth, with D_f. We have also used the Avrami equations to study the gelation of *n*-alkanes by **CNC**[17] at different temperatures and have correlated *n* with D_f. However, it may be inappropriate to compare Avrami-derived D_f values from several systems in which different nucleation mechanisms for LMOGs are involved. For example, although both Liu and co-workers[5c,d] and we[17] studied one-dimensional aggregation processes, Liu found $D_f \approx 2$ in their homogeneous nucleating systems, while we calculated $D_f \approx 1$ in our heterogeneous nucleating ones. The D_f values calculated from the Avrami equations convolute information about the shapes of the objects formed and their mechanism of nucleation.[14] Their specific meaning must be confirmed by other information, such as autosimilarity relationships based on fiber branching.[5c,d]

Here, we calculate mass fractal dimensions (D_f) for the microcrystalline objects in SAFINs of molecular organogels (consisting of an **ALS**-type (**A**romatic-**L**inker-**S**teroid) LMOG, 5α-cholestan-3β-yl *N*-(2-naphthyl) carbamate (**CNC**),[15] or 3β-cholesteryl *N*-(2-naphthyl) carbamate (**CeNC**)) from kinetic data for the first time and investigate the thixotropic properties of the same gels. The fractal analyses are based on a physical model developed by Dickinson[16] and the time-dependent viscoelastic properties of the gel networks are treated according to a stretched exponential model to determine their thixotropic nature.

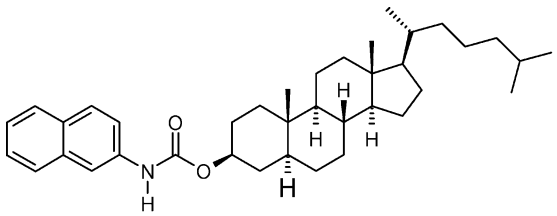

CNC

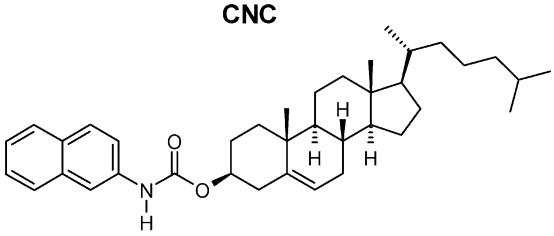

CeNC

Only those **CNC**/*n*-alkane gels prepared by incubation of their sols at temperatures ≤28 °C and, therefore, with spherulitic SAFINs,[17] have been found to be thixotropic; those formed by incubation at ≥30 °C (and with fiberlike SAFINs) remain liquidlike after shearing regardless of the period they are at rest. Both SAFINs rely on one-dimensional growth mechanisms.[18]

Throughout the −8 to 22 °C range of incubation temperatures explored, gels of **CeNC** in ethyl acetate remain liquidlike after shearing and exhibit only fibrous SAFINs by optical microscopy. From other experimental information and the Dickinson model, the D_f values remain 1.1−1.3. However, the Avrami component *n* changes from ca. ∼1 to ∼2 at an incubation temperature of the sol phase near 0.5 °C! These observations add evidence to our assertion that D_f values derived from *n* must be interpreted with caution.

The information provided here demonstrates the importance of controlling the history of molecular gels. Understanding the dynamics of their formation (i.e., history) provides insights into the nature of their aggregate structures and their thixotropic properties, as well as how to reproduce those structures and properties. Unfortunately, many publications have not mentioned the extent to which the properties of molecular gels depend on sample history. Here, we offer a blueprint for how to control and assess the dependence by offering methodologies for treating

(5) (a) Sangeetha, N. M.; Bhat, S.; Choudhury, A. R.; Maitra, U.; Terech, P. *J. Phys. Chem. B* **2004**, *108*, 16056−16063. (b) Singh, M.; Tan, G.; Agarwal, V.; Fritz, G.; Maskos, K.; Bose, A.; John, V.; McPherson, G. *Langmuir* **2004**, *20*, 7392−7398. (c) Liu, X. Y.; Sawant, P. D. *Appl. Phys. Lett.* **2001**, *79*, 3518−3520. (d) Liu, X. Y.; Sawant, P. D. *Adv. Mater.* **2002**, *14*, 421−426.
(6) Barnes, H. A. *J. Non-Newtonian Fluid Mech.* **1997**, *70*, 1−33.
(7) (a) Muthukumar, M. *J. Chem. Phys.* **1985**, *83*, 3161−3168. (b) Muthukumar, M. *Macromolecules* **1989**, *22*, 4658−4660. (c) Wu, H.; Morbidelli, M. *Langmuir* **2001**, *17*, 1030−1036. (d) Shchipunov, Y. A.; Mezzasalma, S. A.; Koper, G. J. M.; Hoffmann, H. *J. Phys. Chem. B* **2001**, *105*, 10484−10488. (e) Ponton, A.; Griesmar, P.; Barboux-Doeuff, S.; Sanchez, C. *J. Mater. Chem.* **2001**, *11*, 3125−3129. (f) Zhong, Q.; Daubert, C. R.; Velev, O. D. *Langmuir* **2004**, *20*, 7399−7405.
(8) Schaefer, D. W.; Martin, J. E.; Wiltzius, P.; Cannel, D. S. *Phys. Rev. Lett.* **1984**, *52*, 2371−2374.
(9) Neimark, A. *Physica A* **1992**, *191*, 258−262.
(10) (a) Wang, M.; Liu, X. Y.; Strom, C. S.; Bennema, P.; van Enckevort, W.; Ming, N. B. *Phys. Rev. Lett.* **1998**, *80*, 3089−3092. (b) Doi, Y.; Tokita, M. *Langmuir* **2005**, *21*, 5285−5289.
(11) Balankin, A.; López, T.; Alexander-Katz, R.; Córdova, A.; Susarrey, O.; Montiel, R. *Langmuir* **2003**, *19*, 362−3634.
(12) For instance, see: (a) Pouzot, M.; Nicolai, T.; Benyahia, L.; Durand, D. *J. Colloid Interface Sci.* **2006**, *293*, 376−383. (b) Pouzot, M.; Nicolai, T.; Durand, D.; Benyahia, L. *Macromolecules* **2004**, *37*, 614−620.
(13) (a) Avrami, M. *J. Chem. Phys.* **1939**, *7*, 1103−1112. (b) Avrami, M. *J. Chem. Phys.* **1940**, *8*, 212−224.
(14) a) Schultz, J. M. *Polymer Materials Science*; Prentice Hall: Englewood Cliffs, NJ, 1974; p 385. (b) Wunderlich, B. *Macromolecular Physics*; Academic Press: New York, 1976; Vol. 2, pp 16−52, 147.
(15) Lu, L.; Cocker, M.; Bachman, R. E.; Weiss, R. G. *Langmuir* **2000**, *16*, 20−34.
(16) Dickinson, E. *J. Chem. Soc., Faraday Trans.* **1997**, *93*, 111−114.
(17) Huang, X.; Terech, P.; Raghavan, S. R.; Weiss, R. G. *J. Am. Chem. Soc.* **2005**, *127*, 4336−4344.
(18) (a) Hench, L. L.; West, J. K. *Chem. Rev.* **1990**, *90*, 33−72. (b) Brinker, C. J.; Scherer, G. W. *Sol-Gel Science*; Academic Press: San Diego, CA, 1989.

Table 1. Gelation Tests of Liquids with 1 wt % **CNC** and **CeNC** as LMOGs[a]

liquid	**CNC**[b]	**CeNC**[b]
methanol		P
ethanol	I	G (3 wt %, <1 week; 88.0−90.7 °C)
1-propanol	P	G (>1 week; 35.1−42.5 °C)
1-butanol	P	G (>1 week; 30.0−30.5 °C)
1-pentanol	P	G (>1 week; 38.0−38.8 °C)
1-octanol	P	G (3 wt %, >1 week; 59.1−71.5 °C)
n-octane	G (<1 week; 40.5−56.2 °C)	P
n-decane	G (<1 week; 46.7−63.8 °C)	P
n-dodecane	G (<1 week; 53.0−53.5 °C)	P
cyclohexane	G (3 wt %, >5 months; 47.1−74.2 °C)	P
benzene	S	S
acetonitrile	P	P
ethyl acetate	P	G (2 wt %, <1 week; 38.0−40.2 °C)
chloroform	S	S

[a] All sols were cooled to room temperature (22 °C) in air. [b] G, gel; P, precipitate; I, sample insoluble when the liquid was heated to boil; S, soluble. Values in parentheses are periods during which gels are stable in sealed vessels at room temperature and the T_g values determined by the inverse-flow method.[19]

the data and, from them, obtaining detailed insights into the self-assembly processes responsible for the construction of the SAFINs.

Results and Discussion

All experimental procedures and analyses, including syntheses and characterizations, are included in the Supporting Information.

Gelation Studies and Gel Structures from Optical Micrographs and Powder XRD. Table 1 summarizes results from gelation studies with **CNC** and **CeNC** as the LMOGs. Qualitatively, gelation was considered successful if no sample flow was observed upon inverting the container at room temperature (i.e., the "inverse flow" method[19]) after a third heating-and-cooling cycle. See Table 2 of Supporting Information and refs 17 and 15 for additional data. The gelation abilities of **CNC** and **CeNC** are very different although they are structurally very similar. The double bond at C5 forces the B-ring of the steroid part of **CeNC** to adopt a boat conformation, and that change affects the overall shape of the molecule (Figure 1).[20]

CNC/*n*-alkane sols, when cooled rapidly to 0 °C and incubated there, are known to yield gels with SAFINs in the form of highly branched, small fibers in spherulitic aggregates.[17] The diameters of the spherulitic assemblies of the gel become larger with increasing incubation temperature, and SAFINs of gels made by incubation of sols between ∼ 35 and 40 °C are nonspherulitic, long fibrous assemblies. With time, the gels with spherulitic (colloidal-type) SAFINs phase-separated into very long fibers whose diffraction pattern is the same as that of the fiberlike neat solid.

Powder XRD patterns of the spherulitic gel, the fiberlike gel, their xerogels, and the spherulitic and fiberlike neat solids are shown in Figure 2. **CNC** xerogels were prepared by drying fresh **CNC**/*n*-octane gels (defined as samples within 5 h of initial cooling) under a dynamic reduced pressure of 440 Torr for several days. This process yielded samples that were not thoroughly dried, as indicated by a broad peak around 20° in 2θ in XRD patterns and thermal gravimetric analyses (TGA). The needlelike **CNC** (Figure 3) crystallized from ethyl acetate exhibits mp 184.1−184.9 °C (lit.[15] mp: 178−180 °C) and a very sharp melting endotherm with a heat flow maximum at 185.4 °C by DSC (Figure 2 of the Supporting Information). Crystals of **CNC** obtained from acetonitrile are spherulitic, with mp 167.9−180.0 °C and a broader endotherm centered at 179.0 °C by DSC.

Various attempts to obtain single crystals of **CNC** (and **CeNC**) failed, so that the actual packing of the molecules within either morph is unknown. However, XRD studies demonstrate that the spherulitic SAFINs and the neat spherulitic solid have the same lamellar packing: the angle ratios of the second through sixth low angle peaks, with respect to the lowest angle one at 1.96°, are 1:1, 2.1:1, 3.0:1, 4.1:1, 5.1:1, and 6.0:1.[21] There may be some interdigitation, perhaps combined with molecular tilting with respect to the lamellar planes, because the estimated extended molecular length of a **CNC** molecule is 27 Å (based on the 3D models in Figure 1) and the lowest angle diffraction corresponds to a Bragg distance of 43.4 Å;[15] interdigitation of other **ALS** gelators within their SAFINs has been reported.[2a,c,d,22] The gels with fiberlike SAFINs have the same XRD diffraction patterns as the fiberlike solids. Although polymorphism is relatively common in LMOGs, there are few examples in which more than one morph leads to gels and, as is the case with **CNC**, where the morph of the SAFIN made from one sol can be changed simply by modifying the cooling protocols.[17,23]

CeNC crystallizes from 1/4 (v/v) ethyl acetate/hexane into tapelike objects (Figure 3c). Only fiberlike SAFINs were found when sols of **CeNC**/ethyl acetate were incubated at temperatures ranging from 0 to 22 °C. Macroscopic phase separation and crystallization into fibers whose molecular packing is the same as that in the gel SAFINs (Figure 4) occur when the incubation temperature is above 25 °C. Thus, there is no evidence of polymorphism in SAFINs of **CeNC**/ethyl acetate gels.

Spectral Studies of CNC and CeNC Aggregation Behavior. Dilute solutions of **CNC** and **CeNC** have similar UV−vis absorption spectra, as expected. Above 300 nm (where reliable data could be obtained over large concentration ranges), the shapes of the spectra remained almost unchanged as the concentration of the LMOG was increased, including at concentrations where gelation was observed (see Figure 5c and Figure 3 of the Supporting Information). The emission spectra are independent of excitation wavelength and remained similar in shape as the LMOG concentrations were increased (Figure 3 of Supporting Information). Although both the excitation and

(19) Eldridge, J. E.; Ferry, J. D. *J. Phys. Chem.* **1954**, *58*, 992−995.
(20) (a) Shieh, H.; Hoard, L, G.; Nordman, C. E. *Acta Crystallogr.* **1981**, *B37*, 1538−1543. (b) Hsu, L.; Kampf, J. W.; Nordman, C. E. *Acta Crystallogr.* **2002**, *B58*, 260−264. (c) Bernal, J. D.; Crowfoot, D.; Fankuchen, I. *Philos. Trans. R. Soc. London, Ser. A* **1940**, *239*, 135−182.
(21) Drits, V. A.; Tchoubar, C. *X-Ray Diffraction by Disordered Lamellar Structures*; Springer-Verlag: Berlin, 1990.
(22) Murata, K.; Aoki, M.; Suzuki, T.; Harada, T.; Kawabata, H.; Komori, T.; Ohseto, F.; Ueda, K.; Shinkai, S. *J. Am. Chem. Soc.* **1994**, *116*, 6664−6676.
(23) Furman, I.; Weiss, R. G. *Langmuir* **1993**, *9*, 2084−2088.

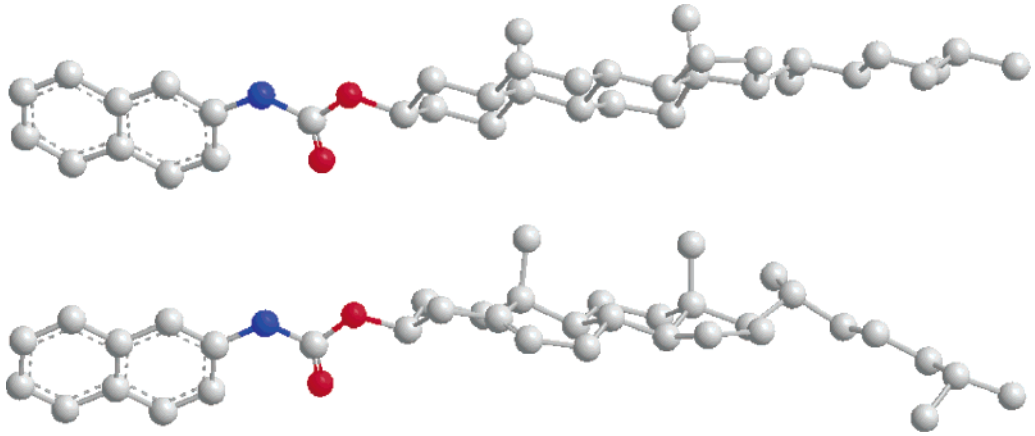

Figure 1. Structures of **CNC** (upper) and **CeNC** (lower), generated by Chem3D Ultra 8.0 (H atoms absent). Only steroidal (S) parts are shown in their lowest energy conformations (minimized by the MOPAC PM3 method); the other A and L parts are presented to emphasize the structural similarities and differences.

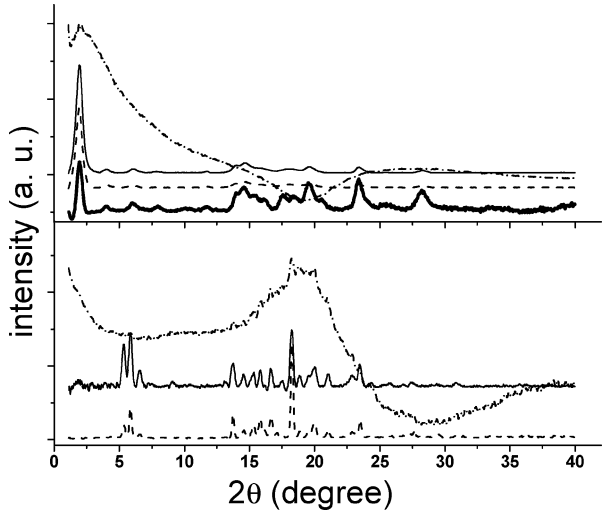

Figure 2. Powder XRD patterns of **CNC**. Upper: neat solid from acetonitrile (—), a 3.0 wt % in *n*-octane gel formed by incubation of a sol at 25 °C (— • — • —) and xerogels from a 3.0 wt % in *n*-octane gel formed at 25 (— —) and 0 °C (— — —). Lower: neat solid from ethyl acetate (— — —), 1.0 wt % **CNC**/*n*-octane gel formed by incubation of a sol at 40 °C (— • — • —) and its corresponding xerogel (— —). The approximate contributions of the liquids have been subtracted empirically[24] from the gel diffraction patterns.

emission spectra of the **CNC**/*n*-octane gel are red-shifted with respect to their solution spectra (by 10 and 7 nm, respectively), those of **CeNC**/ethyl acetate are not. The maxima of the latter remain at 336 nm (excitation) and 356 nm (emission).

However, significant changes in the shape and intensities of the CD spectra were observed as a consequence of the increased chiral organization that accompanied aggregation,[25] and several of these features were sensitive to the manner in which the gels were formed from their sols.

Figure 5a and 5b contain CD spectra of various phases of **CNC** with ethyl acetate or *n*-octane as the liquid. At very low concentrations, only very weak negative CD signals (near 330 nm) are observed because the molecules are not aggregated and their chromophores are far from the chiral centers on the steroidal parts; induced CD is inversely proportional to the third power of the distance between a chromophore and an optically active center.[26] With increasing concentration (and, thus, aggregation), significant increases in the CD signal are observed. In ethyl acetate, a nongelated liquid by **CNC**, the negative CD signals around 318 and 333 nm increase initially as **CNC** concentrations are increased to ca. 0.3 wt % and decrease thereafter (eventually becoming positive). In *n*-octane, a lower polarity and gelated liquid by **CNC**, the CD spectra of solutions below 0.25 wt % are similar to those in dilute (<0.3 wt %) ethyl acetate solutions. **CNC** precipitates from *n*-octane sols at concentrations above 0.3 wt % and forms gels above 0.9 wt %. As the concentration of **CNC** is increased in ethyl acetate or *n*-octane, its chiral aggregates produce much stronger CD spectra and different phases as well. In addition, CD spectra of **CNC**/*n*-octane gels are dependent on the temperature at which their sols were incubated. When 1.0 wt % sols are incubated at ~35—40 °C, gels with fiberlike SAFINs are formed. Their CD spectra have stronger negative bands at 321 and 336 nm (~3 nm red shift from 318 and 333 nm; ^1L_b bands of naphthyl groups[27]) than the corresponding gels formed by incubation at lower temperatures, and a new negative band appears at 303 nm. The origin of the CD band at 303 nm—it is also present, although less prominent, in absorption spectra (Figure 3a of Supporting Information)—is probably related to excitonic coupling by stacked naphthyl groups.[27] The spectrum of the gel with a spherulitic SAFIN, formed by incubation of a sol at 5.4 °C (Figure 5b), for example (see Figure 4 of the Supporting Information for spectra from gels incubated at temperatures in the range from 5.4 to 40.0 °C), shows a positive Cotton effect at ca. 340 nm, indicating the different packing arrangement of **CNC** molecules in the gels with fiberlike SAFINs. For a clearer comparison, molar ellipticities $[\theta]$[27] of the gels are plotted versus **CNC** concentration (Figure 5d).

The differences between both the gelation abilities of the two gelators and the way they organize within their SAFINs are apparent from their CD spectra. As noted in Figure 5a, the sign of the CD bands of **CNC** in ethyl acetate changes from negative to positive as the concentration (and aggregation) increases,

(24) Ostuni, E.; Kamaras, P.; Weiss, R. G. *Angew. Chem., Int. Ed. Engl.* **1996**, *35*, 1324—1326.
(25) (a) Brizard, A.; Oda, R.; Huc, I. *Top. Curr. Chem.* **2005**, *256*, 167—218 and references within. (b) Ciferri, A. *Liq. Cryst.* **1999**, *26*, 489—494. (c) Brunsveld, L.; Vekemans, J. A. J. M.; Hirschberg, J. H. K. K.; Sijbesma, R. P.; Meijer, E. W. *Proc. Natl. Acad. Sci. U.S.A.* **2002**, *99*, 4977—4982.
(26) Craig, D. P.; Power, E. A.; Thirunamachandran, T. *Chem. Phys. Lett.* **1974**, *27*, 149—153.
(27) Harada, N.; Nakanishi, K. *Circular Dichroic Spectroscopy: Exciton Coupling in Organic Stereochemistry*; University Science Books: Mill Valley, CA, 1983; pp 41—43.

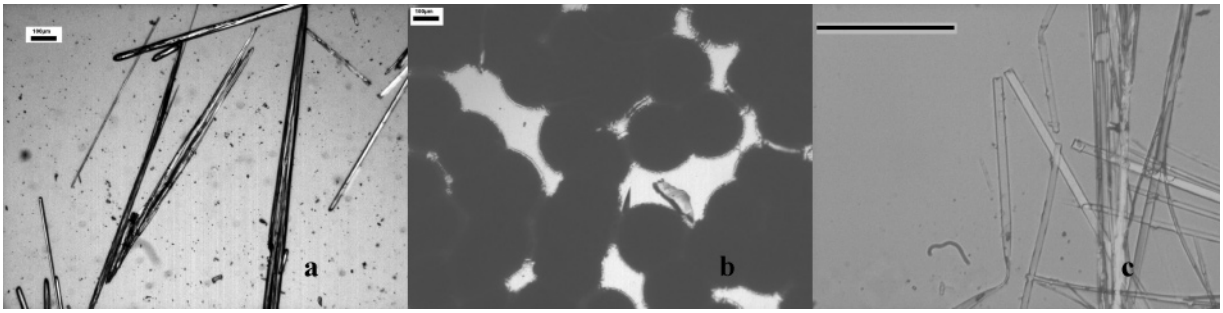

Figure 3. Optical micrographs of **CNC** neat solids recrystallized from (a) ethyl acetate and (b) acetonitrile solutions and (c) **CeNC** neat solids from 1/4 (v/v) ethyl acetate/hexane. Scale bars = 100 μm.

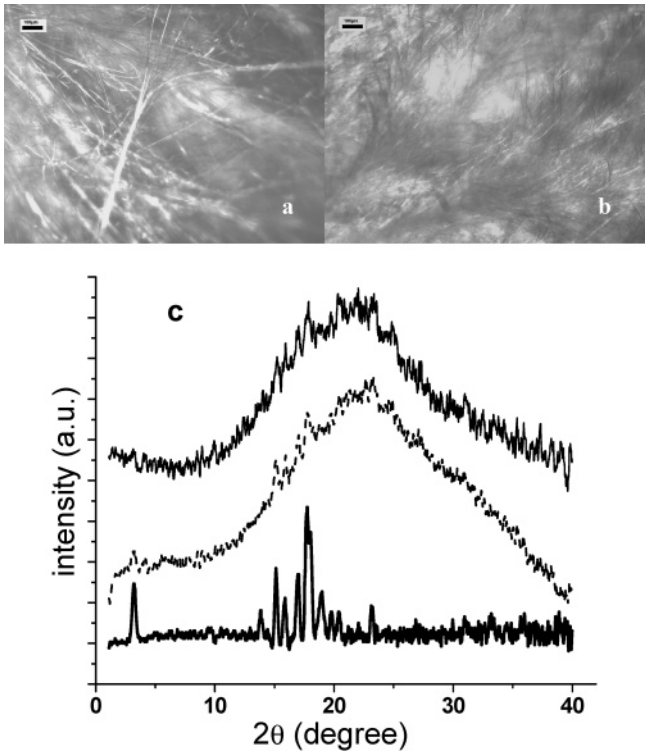

Figure 4. Optical micrographs of 2.0 wt % **CeNC**/ethyl acetate gels formed by cooling sols in air at 22 °C (a) and in an ice−water bath (b); scale bars = 100 μm. (c) Powder XRD patterns of **CeNC** neat crystals from 1/4 (v/v) ethyl acetate/hexane (—) and gels of 2.0 wt % **CeNC**/ethyl acetate formed from sols left at room temperature (− − −) and in an ice−water bath (−−) after subtracting empirically[24] the approximate contributions of the liquid.

without discernible changes in peak positions; **CeNC** precipitates from ethyl acetate sols at concentrations above 0.5 wt % and forms gels above 2.0 wt % at room temperature. Those peak positions correspond to the wavelengths of the band maxima in the absorption spectra. At equivalent dilute (0.05 wt %; 8.12 $\times$ 10^{-4} M) concentrations in ethyl acetate, the molar ellipticities of the 333 nm bands from both **CeNC** and **CNC** are comparable and negative (ca. −46 000 and ca. −34 000 mdeg cm^{-2} mol^{-1}, respectively; Figure 5d), and the ellipticities become positive as the concentration is increased (Figure 5c). The molar ellipticities of the 318 nm bands from both **CNC**/*n*-octane and **CeNC**/ethyl acetate sols show similar trends. Thus, the change in sign of the CD bands does not depend on gelation because only **CeNC** forms a gel in ethyl acetate. However, there are significant wavelength shifts during the gelation of **CeNC** that are not very sensitive to the incubation temperature of its ethyl acetate sols (Figure 5c). These observations are consistent with the previously cited OM and powder XRD results indicating that the SAFINs of the **CeNC** gels are similar, regardless of the protocol used for their formation, and that the molecular packing within gel fibers is chiral (and probably helicoidal).[28] Because no gels are obtained from **CNC** in ethyl acetate, it is difficult to compare their CD spectra and those of **CeNC** at the same higher concentrations. However, it is interesting to note that the CD spectra of **CNC** in *n*-alkanes also exhibit strong positive features near 340 nm and large spectral shifts, but only when incubated at low temperatures (Figure 5b).[17] It is for that reason that the molar ellipticities for gels of **CNC**/*n*-octane were very different when their sols are incubated at 5 and 40 °C while the ellipticities for the gels of **CeNC**/ethyl acetate were nearly the same when their sols are incubated at 0 and 22 °C (Figure 5d).

Dickinson Model for Fractal Analyses and Its Adaptation to CNC/*n*-Alkane and CeNC/Ethyl Acetate Organogels. Analysis of the fractal nature of our molecular organogels is based upon a kinetic model developed by Dickinson.[16] A key feature of it is the time-dependent increase of excluded volume of the aggregates. The model requires that several conditions, which should apply to **CNC** and **CeNC** organogels, be met. They include the following: (1) the gels, once formed, have networks that persist in a steady state; (2) the LMOG aggregates act like hard, uncompressible particles; (3) the cross-sections of the LMOG aggregates are monodisperse or nearly so in size at each length scale and have similar shapes over several length scales; and (4) the kinetics of gelation follows the Smoluchowski model for diffusion.[29] More importantly, the model is based on the formation of two types of bonds, those that are "irreversible" fractal-type and those that are noncovalent and reversible. There may be different strengths of interactions which contribute to the stabilization of the aggregates in the percolating molecular organogel. Under these conditions mentioned above, eq 1 should be applicable to calculate the fractal dimensions of the SAFINs in our molecular organogels. For a derivation of eq 1, see Appendix 1 in the Supporting Information. C is a constant, and ϕ_{eff}^{t}, the effective volume fraction of aggregates at time = t, can be replaced by its corresponding bulk parameter, the volume fraction of the gel phase ϕ_{g}^{t}. In turn, ϕ_{g}^{t} can be expressed by other experimental parameters, such as scattering intensity, G', etc.

$$\ln \phi_{\mathrm{eff}}^{t} = C + (3 - D_{\mathrm{f}})/D_{\mathrm{f}} \ln t \qquad (1)$$

The equations used to analyze the temporal rheological data

(28) Kasha, M. *Rev. Mod. Phys.* **1959**, *31*, 162−169.
(29) Ziff, R. M.; McGrady, E. D. *J. Chem. Phys.* **1985**, *82*, 5269−5274.

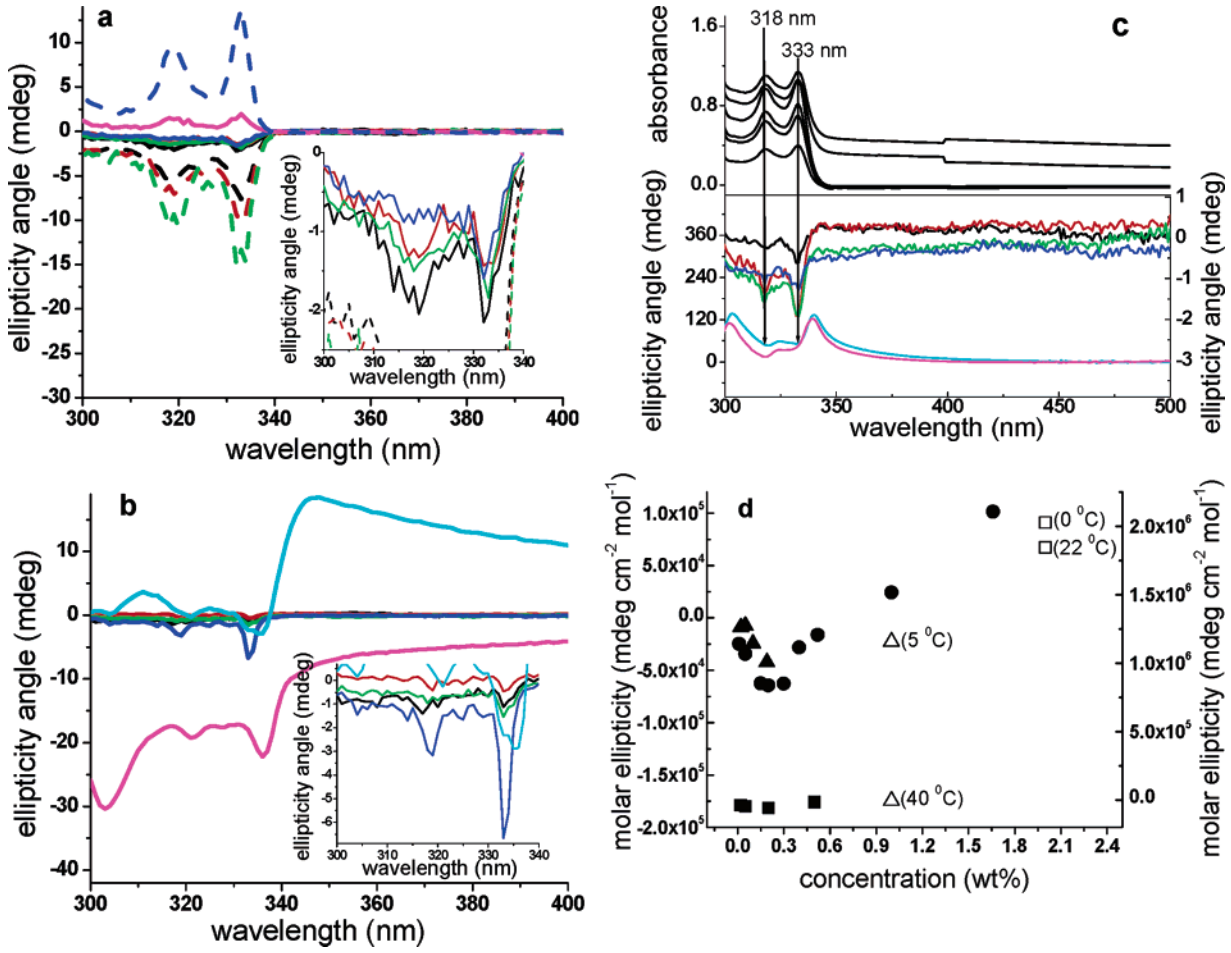

Figure 5. (a) Room-temperature CD spectra of **CNC**/ethyl acetate solutions/sols: 0.01 wt % in a 50 mm length cell and (black solid line), 0.05 (red solid line), 0.15 (black dashed line), 0.2 (red dashed line), 0.3 (green dashed line), 0.4 (green solid line), 0.52 (blue solid line), 1.0 (pink solid line), and 1.66 wt % (blue dashed line) in 5 mm length cells. (b) Room-temperature CD spectra of 0.02 (black solid line), 0.05 (red solid line), 0.1 (green solid line), and 0.25 (blue solid line) wt % **CNC**/*n*-octane solutions/sols and 1.0 wt % gels formed by incubating sols at 40 (pink solid line) or 5 °C (green solid line); cell lengths are 50, 10, 5, 5, 1, and 1 mm, respectively. The insets in (a) and (b) are expansions of the spectra near 0 mdeg. (c) Lower: Room-temperature CD spectra of 0.02 (black solid line), 0.05 (red solid line), 0.2 (green solid line), and 0.5 wt % (blue solid line) **CeNC**/ethyl acetate solutions/sols (right *Y*-axis) and 2.0 wt % gels (left *Y*-axis) formed by incubation of sols at 0 (pink solid line) and 20 °C (green solid line); cell lengths are 5, 5, 1, 0.2, 0.2, and 0.2 mm, respectively. Due to the opacity of the gel samples, the baselines of the recorded CD spectra were negative; they have been offset at the longest wavelengths to move the baselines to 0. Upper: Room-temperature absorption spectra (offset vertically) of 0.02, 0.05, 0.2, and 0.5 wt % **CeNC**/ethyl acetate solutions/sols and 2.0 wt % gels formed by incubation of sols at 0 and 20 °C (from bottom to top); cell thicknesses are 10, 10, 1, 1, 0.2, and 0.2 mm, respectively. (d) Molar ellipticities of **CNC**/ethyl acetate (●), **CNC**/*n*-octane (▲), and **CeNC**/ethyl acetate (■) sols at 333 nm and gels of **CNC**/*n*-octane (△) at 336 nm and **CeNC**/ethyl acetate (□) at 340 nm versus gelator concentration. Incubation temperatures for the gel samples are noted in parentheses.

are stretched exponentials, eqs 2 and 3, in which τ is a time constant representing the recovery speed and m is a dimensionless constant; The G' in eqs 2 and 3 can be other rheological parameters, such as G'', the complex viscosity η^*, etc.

$$G'(t) = G'(0) + [G'(\infty) - G'(0)](1 - e^{-(t/\tau)^m}) \quad (2)$$

$$\ln\left[-\ln \frac{G'(\infty) - G'(t)}{G'(\infty) - G'(0)}\right] = m \ln t - m \ln \tau \quad (3)$$

The kinetics of gelation of **CeNC**/ethyl acetate is also analyzed here using an Avrami equation (eq 4). It has been applied previously to explore the growth kinetics of SAFINs of molecular organogels.[6,17] In this equation, K is a temperature-dependent parameter, similar to a rate constant, and n is the so-called Avrami component that reflects the type of growth leading to phase separation. Note that eqs 2 and 3 are similar in form to eq 4. The parameter m in eq 3 and the Avrami component n are clearly related based on the similarity between the two equations.

$$\ln[-\ln(1 - \phi_g^t)] = n(\ln K + \ln t) \quad (4)$$

Fractal Analyses Based on Kinetic Experiments. The time-dependence of the transformations of **CNC**/*n*-alkane sols to gels has been followed by SANS, rheology, CD, and fluorescence techniques. In each set of experiments, a different characteristic variable of the systems (X) was measured as a function of time: by SANS, the increase of total intensity of scatter collected in a solid angle over a 0.008−0.1 Å^{-1} range of Q; by rheology, the increase of the storage modulus G' (or, in some cases, the loss modulus G''); by CD, the increase of negative band intensities at 303 and 336 nm (incubation at 35.0 and 40.0 °C) or of positive band intensities at 343−347 nm (incubation below 30 °C); by fluorescence, the increase of emission intensity at 375 nm with excitation at 318 nm.

Since the fraction of the gel phase at time = t, $\phi_g^t = [X(t) - X(0)]/[X(\infty) - X(0)]$, can be expressed in terms of X at different

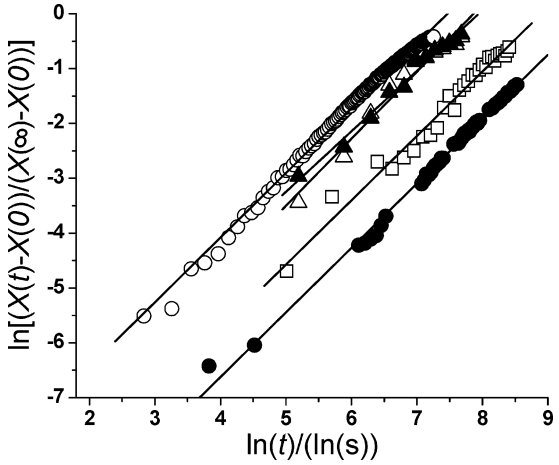

Figure 6. Plots of data according to eq 1 for gelation of sols of 1.0 wt % **CNC**/*n*-octane incubated at 40 °C: rheology G' (○, slope = 1.18, D_f = 1.38, R^2 = 0.997; *n*-dodecane as liquid), SANS (●, slope = 1.18, D_f = 1.38, R^2 = 0.996; *n*-dodecane-d_{26} as liquid), fluorescence (□, slope = 1.17, D_f = 1.38, R^2 = 0.988), and CD at 304 nm (△, slope = 1.22, D_f = 1.35, R^2 = 0.982) and at 336 nm (▲, slope = 1.11, D_f = 1.42, R^2 = 0.993). In the Y-axis, X is the variable quantity being plotted.

times as $X(0)$, $X(t)$, and $X(\infty)$, D_f can be extracted from eq 1 by plotting $\ln\{[X(t) - X(0)]/[X(\infty) - X(0)]\}$ versus $\ln t$ (Figure 6). $X(0)$ and $X(\infty)$ must be determined accurately in order to extract meaningful values of D_f. To do so, $X(\infty)$ has been calculated as the average of the last several data points at times after which no perceptible change could be discerned, at least over a time scale commensurate with the large changes; no attempt was made to include effects from hysteresis. Due to the stochastic nature of the initial nucleation, an irreproducible induction period, which is influenced by the incubation temperature (N.B., longer at higher temperatures) and the technique applied, is usually observed before intensities begin to change. Therefore, $t = 0$ for initial gel formation is considered to be when X begins to change rapidly from its initial value. As such, the exact $t = 0$ is somewhat subjective and has more error potentially than $t = \infty$. $X(0)$ is defined as either the average of X during the induction period or the value of X at the experimental zero time in the absence of a clear induction period. The uncertainty in both values probably contributes to the slight curvature in plots of the kinetic data. In order to determine the influence of these uncertainties on the calculated values of D_f, data treatments in which "zero time" was advanced or retarded by 10% were compared; the deviations from the reported values are small (Table 3 of the Supporting Information).

Data from SANS measurements taken at 40 °C on a sample consisting of 3 wt % **CNC** in *n*-dodecane-d_{26} are not shown in Figure 6 (see Supporting Information Table 7) because the rate of gelation is too rapid to allow a precise calculation of the slope; gelation was complete within <10 min according to the count intensities. Supporting Information Figure 10 shows plots of intensity versus Q counts collected for 10 s periods at different times after the 1.0 wt % sample as a sol had been incubated at 40 °C. The time range encompasses scattering curves from the very early stages to virtually full gel development. Although the signal-to-noise improves with time, the shapes of the curves are similar throughout. The plot at time ~9 h demonstrates the quality of the data; 2 oscillations are observable in spite of the very short collection period.

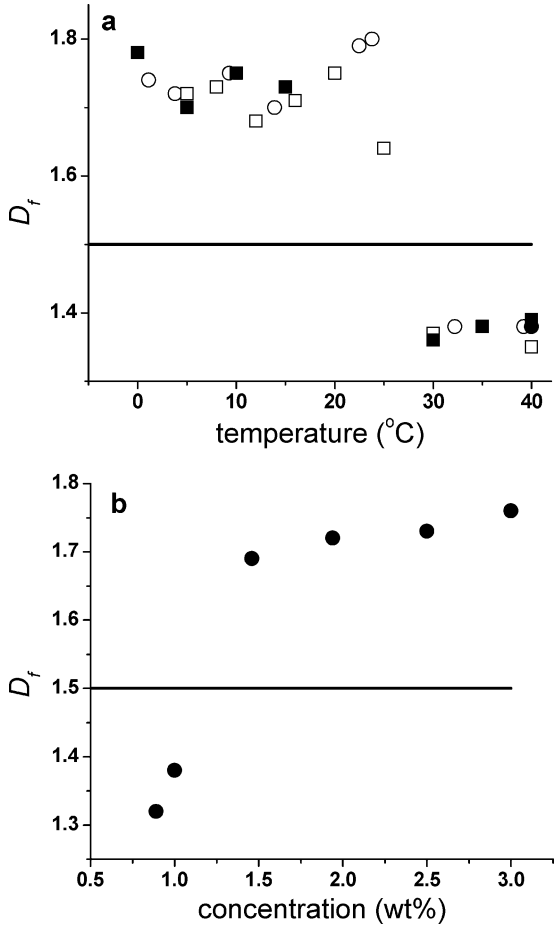

Figure 7. (a) D_f values versus sol incubation temperatures for 1.0 wt % **CNC**/*n*-alkane gels from fluorescence (○, *n*-octane), SANS (●, *n*-dodecane-d_{26}), CD (□, *n*-octane), and rheology G' (■, *n*-dodecane) data. (b) D_f values of **CNC**/*n*-octane gels versus gelator concentration from data obtained during fluorescence experiments on sols incubated at 32.2 °C.

At all temperatures investigated, D_f values are between 1 and 2 (Tables 3 and 4 of the Supporting Information), indicating that **CNC** molecules undergo one-dimensional aggregation and growth during gelation.[18] This conclusion is also reached by treating the data according to Avrami theory[17,13] and by the presence of fiber units, even for SAFINs whose micron-range aggregate units are spherulitic (Figure 6 of the Supporting Information). It is important to note that the existence of an autosimilarity relationship characterized by a fractal dimension is not apparent in treatments of the neutron scattering data from the **CNC** organogel. SANS measurements in the 0.004−0.3 Å^{-1} Q-range (not shown) contain scattering features typical only of the form factor of one-dimensional species with monodisperse cross-sections.[30] The absence of the characteristic fractality features suggests that they should be observed at much smaller Q-values (N. B., the large-Q cutoff is expected to be <0.001 Å^{-1} while the cutoff distance describing the pair correlation function at large distances, in the micron domain where optical viewing is possible, would be at Q < 0.0001 Å^{-1}) in an I versus $Q-D_f$ scattering function.[31]

Figure 7 contains plots of the temperature and concentration dependence of D_f values obtained from eq 1. For 1.0 wt % gels formed by incubation of sols above and below 30 °C, D_f is ca.

(30) Terech, P.; Weiss, R. G., unpublished results.
(31) Teixeira, J. *J. Appl. Crystallogr.* **1988**, *21*, 781−785.

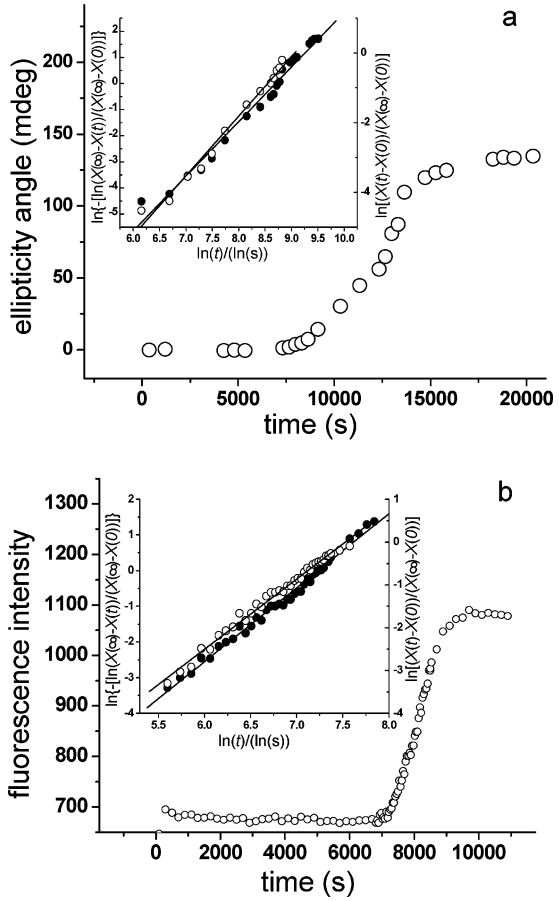

Figure 8. Kinetic studies of 2.0 wt % **CeNC**/ethyl acetate gel formation by following (a) CD intensity increases (340 nm) at 20.2 °C; the inset contains linear fits of the data based on the Avrami model (eq 4; ●, left *Y*-axis; $n = 2.09$, $R^2 = 0.990$) and fractal model (eq 1; ○, right *Y*-axis; slope = 1.71, $D_f = 1.10$, $R^2 = 0.992$) and (b) fluorescence intensity increases (358 nm) at 20.5 °C; the inset contains linear fits of the data based on the Avrami model (eq 4; ●, left *Y*-axis; $n = 2.07$, $R^2 = 0.996$) and fractal model (eq 1; ○, right *Y*-axis; slope = 1.64, $D_f = 1.14$, $R^2 = 0.995$).

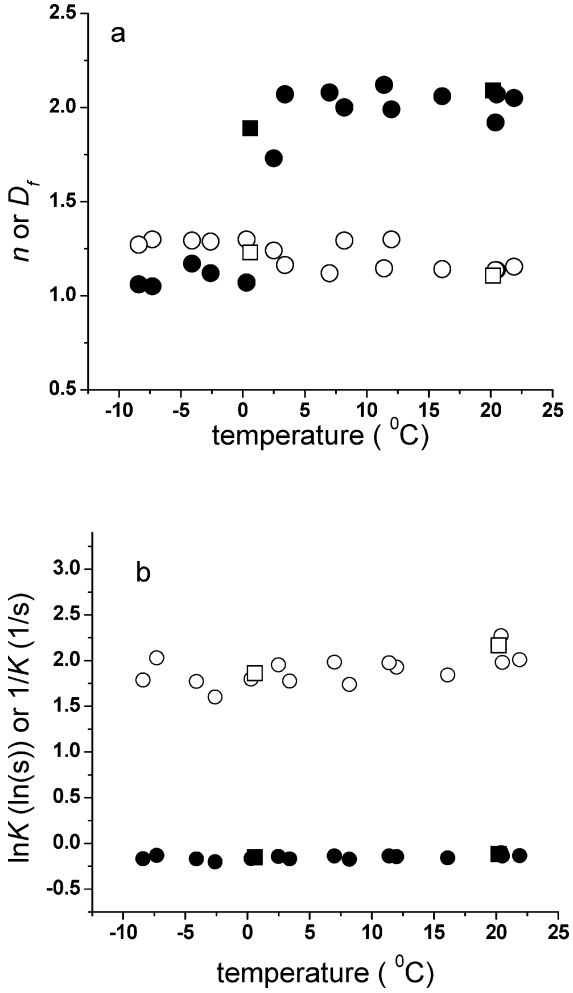

Figure 9. Analyses of data from 2.0 wt % **CeNC**/ethyl acetate samples. (a) Values of the Avrami component *n* (●,■) and D_f (○,□) versus temperature from fluorescence (●,○) and CD (■,□) data; (b) Values of the Avrami 1/*K* (●,■) and ln *K* (○,□) versus temperature from fluorescence (●,○) and CD (■,□) data.

1.3−1.4 and 1.6−1.8, respectively. Values of D_f between 1 and 1.5 indicate fiberlike SAFINs[18] while values between 1.5 and 2 predict spherulitic SAFIN structures (consisting of smaller fiber objects).[18] At 32.2 °C, D_f values are >1.5 at ≥1.5 wt % **CNC** and are <1.5 when CNC is <1.5 wt % (Figure 7b). As noted previously,[17] gels with fiberlike SAFINs are obtained only over very narrow **CNC** concentration ranges (below 1.5 wt %) and sol incubation temperature ranges (between 30 and 40 °C).

Kinetic Studies of CeNC/Ethyl Acetate Gel Formation Based on Avrami and Fractal Approaches. The transformations of 2.0 wt % **CeNC**/ethyl acetate sols to gels were followed by time-dependent intensity changes in CD (at 340 nm; Figure 8a) and fluorescence (λ_{ex} 333 nm; λ_{em} 358 nm; Figure 8b) signals. The data are treated according to fractal (eq 1) and Avrami models (eq 4). The approximate period required for temperature equilibration after sample transfer in these experiments was less than 30 s since a very small amount of sample was used. The shortest period to complete gelation was 10−15 min. Contributions from linear dichroism in the CD spectra are negligible since only slight changes in CD intensity were detected when samples were rotated by 90°. Data from both techniques produce Avrami components *n* near 2 and fractal dimensions D_f of 1.1−1.2. The temperature dependence of the Avrami parameters *n*, *K*, and D_f for 2.0 wt % **CeNC** in ethyl acetate samples are shown in Figure 9 (Table 5 of the Supporting Information). Very interestingly, a transition of *n* from ∼1 to ∼2 is observed around 2.5 °C as temperature is increased (Figure 9a). This is especially noteworthy because *n* is independent of temperature from 5 to 40 °C in **CNC**/*n*-alkane gel systems although there is a clear change in the SAFIN structure near 30 °C![17] The aforementioned OM and powder XRD data show no apparent differences in the SAFINs of the **CeNC**/ethyl acetate gels within the temperature range where the precipitous change in *n* is observed; it is a consequence of a change in the nucleation mechanism rather than in the growth and structure of the fibers. At incubation temperatures below ca. 0.5 °C, the gelation mechanism is based on *heterogeneous nucleation, interfacial control, and one-dimensional* growth; above ca. 0.5 °C, it is based on *homogeneous nucleation, interfacial control, and one-dimensional* growth.[14] The reason for the two regimes must, in part, depend on the degree of supersaturation which increases at lower incubation temperatures. However, heterogeneous nucleation is usually more important at low supersaturation, and it is difficult to distinguish between these two nucleation mechanisms.[32] Furthermore, since plots of ln *K* or 1/*K* versus temperature (Figure 9b) do not show an abrupt change in the

temperature range investigated, it is reasonable to conclude that the same fiber growth mechanism is operative throughout.

Gels of 2.0 wt % **CeNC**/ethyl acetate are generally weak rheologically and not very stable at elevated temperatures or over long periods. However, they *do* form gels despite their D_f values being very low, 1.1−1.3 regardless of the incubation temperature. These D_f values indicate one-dimensional aggregation and fiberlike SAFINs[18] and are consistent with the OM observations, powder XRD patterns, and Avrami-based calculations.

We also observed that the CD and fluorescence intensities of the once-formed gels remained constant for hundreds to a few thousands of seconds, depending on temperature. However, the intensities decreased (see Figure 7a and 7b of the Supporting Information) thereafter without a corresponding discernible change in optical micrographs of the SAFIN. This behavior is indicative of an annealing process, such as syneresis.[2c]

Thixotropic Properties of CNC/*n*-Alkane Organogels. Previously,[17] we observed that **CNC**/*n*-alkane gels formed by cooling sols in an ice−water bath and at room temperature became fluid when shaken by hand and regelated when left at rest. Gels formed by incubation of sols at 40 °C had stronger networks that could not be destroyed when shaken by hand. Here, we examine the thixotropic properties of 1.0 wt % **CNC**/*n*-dodecane gels, formed by incubation of sols at various temperatures and sheared, using time-dependent rheological measurements, the recovery of G' and G''. **CeNC**/ethyl acetate gels undergo irreversible phase separation upon mechanical agitation.

Rheological experiments were conducted under oscillatory shear, and the storage modulus (G'), the loss modulus (G''), the ratio between G'' and G' ($\tan\delta$), and the complex viscosity (η^*) were measured as functions of frequency, ω. *n*-Dodecane, rather than *n*-octane, was the liquid to minimize evaporation from samples at superambient temperatures, and at a strain of 1% and a frequency of 10 rad/s, which are within the approximate linear viscoelastic (LVE) regime[33] (Figure 1 of the Supporting Information); at 40 °C, slightly below the sol−gel transition temperature, the frequency sweeps indicate that the sample behaves like a soft viscoelastic solid. The gap between the plates (0.3−0.5 mm) did not influence the rheological data, indicating that wall slip was not a factor. Samples were left undisturbed for 30 min to 4 h (based on the nature of the kinetic study) to complete gelation after the temperature, and the gap reached the desired values. The sample was then sheared at a constant shear rate of 2 s^{-1} for 600 s, and immediately afterward, the recovery of G' was monitored. A frequency-dependent sweep was also performed both before shearing and after recovery between 0.01 and 100 rad/s at 1% strain to ascertain whether a "true" gel was present.[34]

Figure 10 shows a typical plot of the increase of G' after shearing a **CNC**/*n*-dodecane gel. Treatment of the data according to eq 3 gives $m = 1$. The inset follows the recovery of G' from

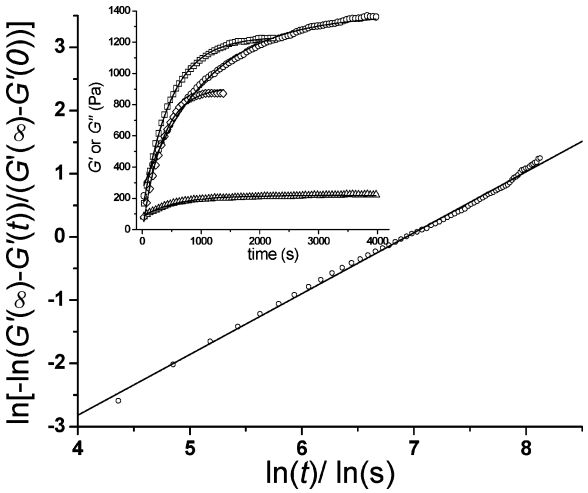

Figure 10. Recovery of G' at 25 °C of a sheared 1.0 wt % **CNC**/*n*-dodecane gel formed from its sol at 25 °C (first run, ○) and the linear best fit of the data according to eq 3 ($m = 1.0$, $R^2 = 0.998$). Inset: recovery of G' (○, first run, $\tau = 1107 \pm 20$ s, $R^2 = 0.997$; □, second run, $\tau = 478 \pm 3$ s, $R^2 = 1.000$; ◇, third run, $\tau = 341 \pm 11$ s, $R^2 = 0.996$) and G'' (△, first run, $\tau = 581 \pm 18$ s, $R^2 = 0.987$) after the gel was sheared and the corresponding single-exponential decay fits according to eq 2 as solid lines.

three consecutive runs and G'' during the first run, where a gel formed from the sol at 25 °C was mechanically disturbed. In each case, the data are fit to an exponential decay function according to eq 2. The similar values of G' and G'' immediately after shearing demonstrate that the gels were destroyed. With progressive shear-recovery cycles, the recovery time decreases, the plateau value G' becomes smaller, and macroscopic phase separation occurs eventually as the SAFINs of the gels become increasingly fatigued due to the cleavage of fibers and their "junction zones".[2] In addition, the spherulites of the original gel change their form to more and more fiberlike SAFIN structures as the number of shear-recovery cycles increases (Figure 11); shear also changes the nature of the SAFIN.[6,35]

These trends are followed by other 1.0 wt % **CNC**/*n*-dodecane gels formed from sols incubated at temperatures ≤28 °C (Figure 8 in the Supporting Information). They are also thixotropic and have $m \approx 1$. The associated τ values are shown in Figure 12 (Table 6 of the Supporting Information). 1.0 wt % **CNC**/*n*-dodecane gels formed from sols incubated at temperatures ≥ 30 °C (Figure 8 of the Supporting Information) do not reestablish their gel states; in essence, they have infinite recovery times. The $1/\tau$ values, including those "assumed" to have zero (i.e., $1/\infty$) values, are plotted versus temperature in Figure 12. The recovery of the gel networks after shearing becomes faster as temperature increases up to 28 °C, and a sharp transition is observed thereafter (consistent with the temperature at which the change of spherulitic to fiberlike SAFINs is observed). The reproducibility of the absolute values of G', G'', and τ are not very good because they are sensitive to factors that are very difficult to control, such as the history of the sample, the presence of nucleating sites (e.g., microparticulates and small scratches on the rheometer plates). However, the trends are clear and reproducible. Since the chemical composition of the samples is the same, the thixotropy changes of the gels must be attributed only to differences in the rates and types of SAFIN formation.

(32) (a) Mullin, J. W. *Crystallization*, 3rd ed.; Butterworth-Heinemann: Oxford, UK, 1992. (b) Jones, A. G. *Crystallization Process Systems*; Butterworth-Heinemann: Oxford, UK, 2002; p 125.
(33) Khan, S. A.; Royer, J. R.; Raghavan, S. R. *Aviation Fuels with Improved Fire Safety: A Proceeding*; National Academy Press: Washington, DC, 1997; pp 31−46.
(34) (a) Almdal, K.; Dyre, J.; Hvidt, S.; Kramer, O. *Polym. Gels Networks* **1993**, *1*, 5−17. (b) Khan, S. A.; Royer, J. R.; Raghavan, S. R. *Aviation Fuels with Improved Fire Safety: A Proceeding*; National Academy Press: Washington, DC, 1997; pp 31−46.
(35) Millers, P. D. A.; Goodwin, J. W.; Grover, B. W. *Colloid Polym. Sci.* **1991**, *269*, 949−963.

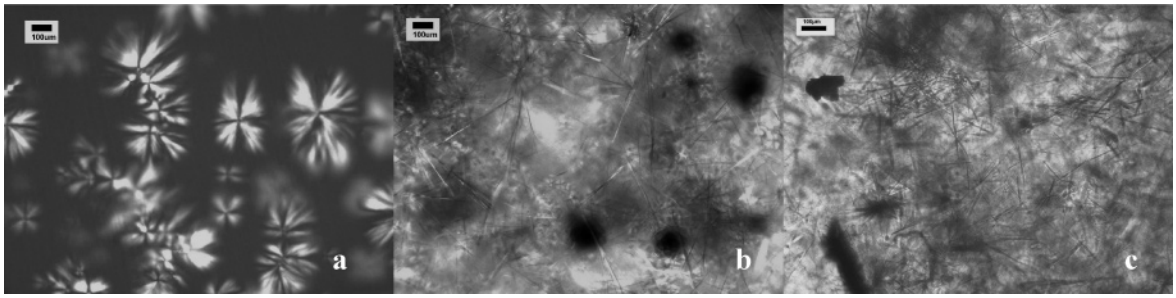

Figure 11. Optical micrographs of a 1.0 wt % **CNC**/*n*-dodecane gel freshly made by incubation of the sol at 25 °C (a) and after recovery from being sheared at 25 °C once (b) and twice (c). Space bars = 100 μm.

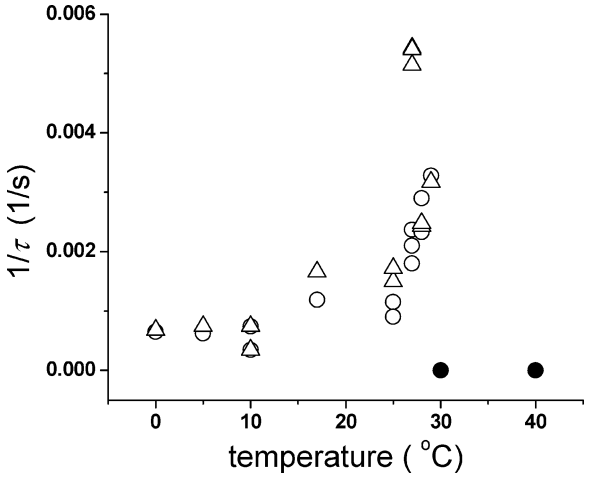

Figure 12. $1/\tau$ for recovery of sheared 1.0 wt % **CNC**/*n*-dodecane gels (first shearing) formed by incubation of their sols at the shear-recovery temperatures shown. The data are from G' (○) and G'' (△). The filled circles are for nongel samples, as indicated by G''/G' remaining >1 over long periods (Figure 8b and 8c of the Supporting Information) and visual phase separation.

Another feature of Figure 12 is that the τ values calculated from the changes in G'' are smaller than those from G'. We believe that the τ values from G' (which is more related with the solid characteristics of a material) are better reporters of the regelation processes than G'' (which is more associated with the liquid properties of a material).[6,42]

Similar shear-recovery experiments were also performed on 3.0 wt % **CNC**/*n*-dodecane gels from sols that had been incubated at 5, 15, and 30 °C. Although they were thixotropic, their recovery curves after shear could not be fitted to single-exponential decay functions, especially at early times (Supporting Information Figure 9). We conjecture that processes which are negligible at low concentrations, such as relaxation from aligned particles,[6] also contribute to the increase of G' and G''.

Based on analyses of more than 250 paints, Pryce-Jones concluded that thixotropy is more pronounced in systems containing nonspherical than spherical particles,[36] and the thixotropy of molecular organogels has been related to SAFINs of interwined and fused fibers[2a,43b,f] or ultrathin, extended, and stable fibers with low crystallinity.[43e,37] Here, the organogels with SAFINs consisting of entangled, long fibers are not thixotropic, while the gels with spherulitic aggregates are. Some form of interactions among the spherulites is necessary for gelation to occur. However, since interactions *among* neighboring spherulites should be weaker than the entanglement interactions *within* a single spherulite, the former is expected to be the primary reason why shear leads to loss of the gel properties as well as why those properties can be restored with time. For related reasons and as noted above, the fatigue observed after several shear-recovery cycles may be associated with the progressive destruction of the spherulites and their transformation into the more stable (but not thixotropic) fiber form of the SAFINs.

Conclusions

The fractal dimensions of SAFINs of molecular organogel systems consisting of **CNC**/*n*-alkane and **CeNC**/ethyl acetate mixtures have been extracted from kinetic data for the first time. The basic conclusions from those studies, especially the dependence of SAFIN structure on incubation temperature of the sol phases, have been confirmed by real space observations involving optical micrography. In addition, rheological experiments have been performed to determine the thixotropic nature of the gels. We note that although thixotropy is an important attribute of some paints, foods, and biological materials (such as actomyosin[38] and blood,[39] tooth enamel growth,[40] cell membrane function[41]),[42] it has been reported for few molecular organogels because of the experimental difficulties associated with obtaining reliable measurements.[43]

Several interesting observations, as well as several important conclusions concerning the gelation mechanisms of LMOG-based systems, have been reported here. Thus, by varying the incubation temperature of its sols and concentration in an *n*-alkane, **CNC** can be directed to either of two types of SAFINs which also correspond to two crystal morphs. At incubation temperatures ≤ 28 °C or **CNC** concentrations above 1.5 wt %, thixotropic gels with spherulitic SAFINs whose D_f values are 1.6−1.8 are formed. Their powder XRD patterns indicate

(36) (a) Pryce-Jones, J. *J. Oil Chem. Assoc.* **1934**, *17*, 305−375. (b) Pryce-Jones, J. *J. Oil Chem. Assoc.* **1936**, *19*, 295−337. (c) Pryce-Jones, J. *J. Oil Chem. Assoc.* **1943**, *26*, 3−13.
(37) Blow, D. M.; Rich, A. *J. Am. Chem. Soc.* **1960**, *82*, 3566−3571.
(38) Waser, P. G. *Science* **1957**, *125*, 739.
(39) We use the word "blood" in a broader sense here. See: Garlaschelli, L.; Ramaccini, F.; Sala, S. D. *Nature* **1991**, *353*, 507.
(40) (a) Eastoe, J. E. *Nature* **1960**, *187*, 411. (b) Du, C.; Falini, G.; Fermani, S.; Abbott, C.; Moradian-Oldak, J. *Science* **2005**, *307*, 1450−1454.
(41) Loor, F. *Nature* **1976**, *264*, 272−273.
(42) Bauer, W. H.; Collins, E. A. In *Rheology: Theory and Application*; Eirich, F. R., Ed.; Academic Press: New York, 1967; Vol. 4, Chapter 8.
(43) (a) Ostuni, E. M.S. Thesis, Georgetown University, Washington DC, 1995. (b) van Esch, J.; Schoobeek, F.; de Loos, M.; Kooijman, H.; Spek, A. L.; Kellogg, R. M.; Feringa, B. L. *Chem.—Eur. J.* **1999**, *5*, 937−950. (c) Terech, P.; Pasquier, D.; Bordas, V.; Rossat, C. *Langmuir* **2000**, *16*, 4485−4494. (d) Lescanne, M.; Grondin, P.; d'Aléo, A.; Fages, F.; Pozzo, J.-L.; Monval, O. M.; Reinheimer, P.; Colin, A. *Langmuir* **2004**, *20*, 3032−3041. (e) Shirakawa M.; Fujita, N.; Shinkai, S. *J. Am. Chem. Soc.* **2005**, *127*, 4164−4165. (f) Loiseau, J.; Lescanne, M.; Colin, A.; Fages, F.; Verlhac, J. B.; Vincent, J. M. *Tetrahedron* **2002**, *58*, 4049−4052. (g) Lescanne, M.; Colin, A.; Mondain-Monval, O.; Fages, F.; Pozzo, J. L. *Langmuir* **2003**, *19*, 2013−2020.

Scheme 1. Cartoon Representation of the Self-Assembly Processes Leading to Our LMOG Gels and the Consequences of Shear on the Spherulitic and Fibrillar SAFIN Morphs

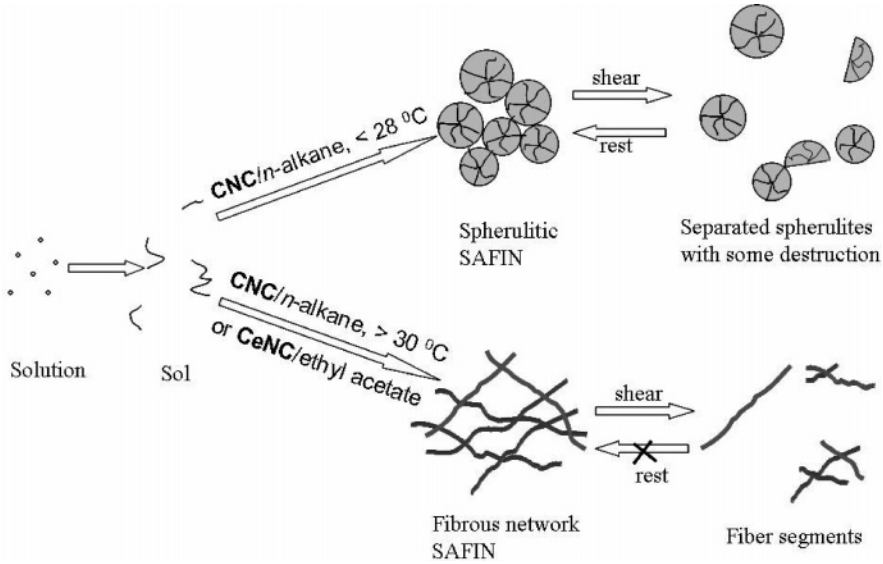

lamellar packing of molecules within the fibers constituting the substructures that is the same as in crystals precipitated from ethyl acetate solutions. **CNC** concentrations of ca. 0.9−1.0 wt % and incubation temperatures of 30−40 °C produce gels with fiberlike SAFINs and D_f values of 1.3−1.4; once sheared beyond their structural limits, they do not recover their gelled states. The D_f values indicate one-dimensional aggregation and are consistent with microscopic observations and conclusions derived from Avrami-type studies.

At all temperatures where gels were formed, Avrami-type kinetic studies suggest "instantaneous nucleation" and one-dimensional growth of SAFINs in **CNC**/*n*-alkane gels.[17] However, these results do not explain why different SAFIN morphs derive from the same type of nucleation and growth mechanism; our fractal studies *do* differentiate the two processes. Thus, a combination of the results from Avrami and fractal treatments of the data reveals a deeper understanding of the processes responsible for SAFIN formation and gelation.

Under all of the experimental conditions employed to form **CeNC**/ethyl acetate gels, only one form of their SAFINs was observed, and fractal analyses yielded D_f values of 1.1−1.3, indicating one-dimensional assembly and fiberlike SAFINs. Surprisingly, the Avrami component *n*, which is normally temperature-independent, changes abruptly with incubation temperatures of **CeNC**/ethyl acetate samples. At 2 wt % **CeNC**, the increase in D_f from ca. 1 below 0.5 °C to ca. 2 above this temperature is probably due to a change in the nucleation mechanism from heterogeneous at lower temperatures to at homogeneous higher temperatures rather than structural changes in the SAFINs; *D_f values derived from the Avrami component n can lead to erroneous conclusions about SAFIN structures* unless they are confirmed by an independent observable.

The essence of these observations and conclusions are summarized in Scheme 1. Transformation of the sols is the critical point in the hierarchy of aggregation steps at which the SAFIN structure of the gels is determined:[44] the sols are dynamic structures which are able to interconvert rapidly with their unaggregated LMOG components. This model requires that the relationships between the rates for LMOG diffusion, nucleation of aggregated species, and growth along specific axes of SAFIN components determine which type of gel structure is eventually formed. Models for differential growth of anisotropic objects in very different systems have been developed[45] and polytropism in crystalline objects is well-established.[46] They can be parametrized to predict the formation of spherulitic or fibrillar objects like the ones obtained here. A future challenge will be to try to fit the empirical rates we have measured to models as a means of determining the form of the actual rate laws and the associated rate constants for gelation.

Regardless, the rheological measurements following the ability of a gel sheared beyond its stress limit to recover its viscoelastic properties have demonstrated the integral link between SAFIN structure and thixotropy in these systems. The correlation between the rheological changes and our real space observations of SAFIN objects before and after shearing lead us to the cartoon in Scheme 1. Gels with spherulitic SAFINs can be transformed into sols via shear without significant destruction of the building blocks of the SAFIN structure; their reassembly can then occur as the spherulites re-entangle.[47] However, shearing the gels with fibrous SAFINS must be accompanied by disassembly of the network and irreversible cleavage of fiber segments into shorter pieces. In the absence of an extraordinary force to "glue" the broken the segments together along the specific axes of the cleavage,[48] the SAFIN cannot be reformed and the viscoelastic properties of the original gel cannot be re-established. These conditions appear to be more

(44) (a) Sakurai, K.; Jeong, Y.; Koumoto, K.; Friggeri, A.; Gronwald, O.; Sakurai, S.; Okamoto, S.; Inoue, K.; Shinkai, S. *Langmuir* **2003**, *19*, 8211−8217. (b) Wang, R.; Geiger, C.; Chen, L.; Swanson, B.; Whitten, D. G. *J. Am. Chem. Soc.* **2000**, *122*, 2399−2400.

(45) (a) Gránásy, L.; Pusztai, T.; Börzsönyi, T.; Warren, J. A.; Douglas, J. F. *Nat. Mater.* **2004**, *3*, 645−650. (b) Granasy, L.; Pusztai, T.; Borzsosnyi, T.; Toth, G. I.; Tegze, G.; Warren, J. A.; Douglas, J. F. *Philos. Mag.* **2006**, *86*, 3757−3778.

(46) For instance, see: (a) Verma, A. R.; Krishna, P. *Polymorphism and polytypism in crystals*; Wiley: New York, 1966. (b) Davey, R. J.; Garside, J. *From Molecules to Crystallizers*; Oxford University Press: New York, 2000 and references cited therein.

(47) For instance, see: Chapters 1 and 6 in ref 2c.

(48) (a) Ostuni, E. M.S. Thesis, Georgetown University, Washington, DC, 1995. (b) Lescanne, M.; Grondin, P.; d'Aleo, A.; Fages, F.; Pozzo, J. L.; Monval, O. M.; Reinheimer, P.; Colin, A. *Langmuir* **2004**, *20*, 3032−3041.

stringent when the SAFINs of molecular organogels are crystalline, as here, than when they are not.[49]

There are already indications from careful studies with *N*-3-hydroxypropyl dodecanamide,[43d] 2,3-di-*n*-decyloxyanthracene,[43g] and a binary gelator of bis(2-ethylhexyl) sodium sulfosuccinate (AOT) and 4-chlorophenol[50] as the LMOGs that the phenomena reported here are more prevalent than generally appreciated. Regardless, it is clear that the dynamics of formation and history of molecular gels must be reported along with their composition. Without such information, it may not be possible for others to reproduce the SAFIN structures and other properties of molecular gels.

In general, gelation with **ALS** gelators depends on a delicate balance among $\pi-\pi$ stacking interactions of aromatic groups, dispersive interactions of steroidal groups, dipolar forces, and H-bonding where possible. Thus, the small differences between the molecular structures of **CNC** and **CeNC** have been shown to result in very different gelation abilities and behaviors. Clearly, the model and approach used here can be applied to many other self-assembling systems, including other molecular gels.[51] It will be interesting to determine whether the results from the fractal model applied here and from real space measurements of the SAFINs correlate in other systems. In that regard, future studies will employ structurally simpler LMOGs.

Acknowledgment. This article is dedicated to Professor Vaidyanathan Ramamurthy on the occasion of his 60th birthday. X.H. and R.G.W. thank the U.S. National Science Foundation for its support of this research. We are grateful to Dr. Gokul C. Kalur and Mr. Bani Cipriano of the Department of Chemical Engineering, University of Maryland, for help in obtaining the rheological data and to Prof. Eric Dickinson of the Procter Department of Food Science at the University of Leeds for discussions about his fractal model.

Supporting Information Available: A detailed Experimental section, an Appendix with a derivation of the fractal equations used, and additional spectroscopic and kinetic data, including tables of D_f, n, and τ values for **CNC**/*n*-alkane and **CeNC**/ethyl acetate gels at several concentrations and temperatures. This material is available free of charge via the Internet at http://pubs.acs.org.

JA0657206

(49) (a) Markovic, N.; Dutta, N. K.; Williams, D. R. G.; Matisons, J. In *Polymer Gels: Fundamentals and Applications*; Bohidar, H. B., Dubin, P., Osada, Y., Eds.; ACS Symposium Series 833; American Chemical Society: Washington, DC, 2003; pp 190−204. (b) Singh, M.; Agarwal, V.; De Kee, D.; McPherson, G.; John V.; Bose, A. *Langmuir* **2004**, *20*, 5693−5702.
(50) Tan, G.; John, V. T.; McPherson, G. L. *Langmuir* **2006**, *22*, 7416−7420.
(51) There are some notable approaches to link the structures of LMOGs, oligopeptides,[51a,b] and amphiphiles,[51c,d] to the hierarchy in the evolution of their hydrogel network (or related phase) structures. However, they emphasize the sequence of that evolution as a function of LMOG concentration without following the actual rates. (a) Aggeli, A.; Nyrkova, I. A.; Bell, M.; Harding, R.; Carrick, L.; McLeish, T. C. B.; Semenov, A. N.; Boden, N. *Proc. Natl. Acad. Sci. U.S.A.* **2001**, *98*, 11857−11862. (b) Chapter 3 in ref 2c. (c) Shimizu, T.; Masuda, M.; Minamikawa, H. *Chem. Rev.* **2005**, *105*, 1401−1443. (d) Fuhrhop, J. H.; Helfrich, W. *Chem. Rev.* **1993**, *93*, 1565−1582.

Supporting Information for

Distinct Kinetic Pathways Generate Organogel Networks with Contrasting Fractality and Thixotropic Properties

*Xiao Huang,[1] Srinivasa R. Raghavan,[2] Pierre Terech,[3] and Richard G. Weiss[1]**

[1]*Department of Chemistry, Georgetown University, 37th and O Streets, NW, Washington, DC 20057-1227, USA,* email: weissr@georgetown.edu
[2]*Department of Chemical and Biomolecular Engineering, University of Maryland, College Park, MD 20742-2111, USA*
[3]*CEA-Grenoble, DRFMC/SI3M Laboratoire Physico-Chimie Moleculaire 17, Rue des Martyrs 28054 Grenoble cedex 9, France*

Experimental section

Materials. *n*-Octane (Aldrich, 98%), *n*-dodecane (Acros, 99+%), *n*-dodecane-d_{26} (MSD Isotopes, 98 atom% D), acetonitrile (Fisher Scientific, HPLC grade) and ethyl acetate (Fisher Scientific, HPLC grade) were used as received. 5α-Cholestan-3β-yl *N*-(2-naphthyl) carbamate (**CNC**) and 3β-cholesteryl *N*-(2-naphthyl) carbamate (**CeNC**), two **ALS**-type (**A**romatic-**L**inker-**S**teroid) organic gelators,**Error! Bookmark not defined.** were synthesized as described in the literature (see below).[1] **CNC** was

recrystallized from ethyl acetate or acetonitrile solutions and **CeNC** was recrystallized from 1/4 (v/v) ethyl acetate/hexane.

Syntheses and characterizations of CNC and CeNC. 3β-Cholesteryl *N*-(2-naphthyl) carbamate (**CeNC**) was synthesized as described in the literature.[2] 0.22 g (1.5 mmol) 2-aminonaphthalene (Aldrich, 95%) was dissolved in 7.5 mL dry benzene with 0.25 mL dried pyridine in a 50 mL round-bottom flask. Then, 0.7 g (1.6 mmol) 3β-cholesteryl chloroformate (Aldrich, 98%), dissolved in 7.5 mL dry benzene, was added dropwise with stirring at 0 ˚C. It was stirred for another 3-4 h, and then extracted with water, saturated aqueous $NaHCO_3$ and water. A yellowish solid was obtained after removal of the liquid using a rotary evaporator under vacuum. The crude product was recrystallized three times from ethyl acetate/hexane (1/4, V/V) to give 0.32 g (38% yield) of white crystals, mp 181.2-183.7 °C (one peak in HPLC with 1/9 ethyl acetate/hexane as eluent). ^{1}H-NMR (300MHz, $CDCl_3$): 7.99ppm, 7.78-7.75ppm, 7.47-7.26 ppm (m, 7H, aromatic), 6.70ppm (s, 1H, NH), 5.43 (s, 1H, C=C-H), 4.67-4.61ppm (m, 1H, CH), 2.46-0.60ppm (m, 44H, cholesteryl). IR (Attenuated total reflectance): 3426 (N-H), 3060 (aromatic, C-H), 1731 (C=O, s), 1644 (C=C) cm^{-1}. Elemental analysis: calcd for $C_{38}H_{53}NO_2$, C 82.11%, H 9.61%, N 2.52%; found, C 81.83%, H 9.90%, N 2.77%.

5α-Cholestan-3β-yl *N*-(2-naphthyl) carbamate (**CNC**) was synthesized similarly (using 5α-cholestan-3β-yl chloroformate) to yield material of mp 184.1-184.9 °C (lit mp 178 - 180 °C[2]; one peak in HPLC with 1/9 ethyl acetate/hexane as eluent). Elemental Analysis:

calcd for $C_{38}H_{55}NO_2$, C 81.82%, H 9.94%, N 2.51%; found, C 81.83%, H 10.38%, N 2.53%. ^{1}H-NMR: 8.00, 7.80-7.72, 7.46-7.28 (m, 7H, aromatic), 6.72 (s, 1H, NH), 4.80-4.65 (m, 1H, CH), 2.20-0.60 ppm (m, 46H, cholestanyl).

Supporting Table 1. Sources and Purities of Liquids for Gelation Tests

Solvent	Purity (from supplier)	Supplier
methanol	99+%	Aldrich
ethanol	200 proof	Warner-Graham
1-propanol	certified	Fisher Scientific
1-butanol	99.5%, spectrophotometric	Aldrich
1-pentanol	certified	Fisher Scientific
1-octanol	99+%	Aldrich
n-octane	98%	Aldrich
n-decane	99+%	Acros
n-dodecane	99+%	Acros
cyclohexane	HPLC	Fisher Scientific
benzene	certified	Fisher Scientific
acetonitrile	HPLC	Fisher Scientific
ethyl acetate	HPLC	Fisher Scientific
chloroform	HPLC	Fisher Scientific

Instrumentation and sample preparations. Samples for gelation studies were prepared by flame-sealing 5 mm (i.d.) glass tubes that contained known amounts of a liquid and gelator. The tubes were heated in a water or oil bath until the gelator dissolved completely. Thereafter, the hot solutions/sols were cooled rapidly to different

temperatures and incubated there until gelation occurred. Qualitatively, gelation was considered successful if no sample flow was observed upon inverting the container at room temperature (i.e., the 'inverse flow' method[3]) after a third heating-and-cooling cycle. Sources and purity of liquids employed in gelation test are listed in Supporting Figure 1.

Optical micrographs (OMs) and melting points were recorded on a Leitz 585 SM-LUX-POL microscope equipped with crossed polars, a Photometrics CCD camera interfaced to a computer, a Leitz 350 heating stage, and an Omega HH503 microprocessor thermometer connected to a J-K-T thermocouple. The samples for optical micrographs were aliquots of gels described above that had been transferred as sols to 0.4 mm thickness flatted capillary tubes (VitroCom) and flame-sealed therein. They were then heated to their solution/sol phase in a boiling water bath and incubated at different temperatures until gelation occurred before the OMs were recorded.

X-ray diffraction (XRD) of samples was performed on a Rigaku R-AXIS image-plate system with Cu Kα X-rays (λ = 1.54 Å) generated by a Rigaku generator operating at 46 kV and 46 mA with the collimator at 0.3 mm. Data processing and analyses were performed using Materials Data JADE (version 5.0.35) XRD pattern processing software. Samples were sealed in either 1.0 mm (gels, exposures for 10 h) or 0.5 mm (neat powder or xerogel, exposure for 15 min) glass capillaries (W. Müller, Schönwalde, Germany). **CNC** xerogels were prepared by drying fresh **CNC**/*n*-octane gels (defined as samples within 5 h of initial cooling) under a dynamic reduced pressure of 440 Torr for several

days. This process yielded samples that were not thoroughly dried, as indicated by a broad peak around 20° in 2θ in XRD patterns and thermal gravimetric analyses (TGA).

Differential scanning calorimetry (DSC) was performed on a TA 2910 differential scanning calorimeter interfaced to a TA Thermal Analyst 3100 controller. All DSC temperatures are reported at maximum heat flow. Heating rates were 5 °C/min; cooling rates were variable and depended on the difference between the cellblock and ambient temperatures.

Kinetics of gelation by CD spectroscopy. **CNC**, dissolved in hot *n*-octane, was transferred to a 1.0 mm thick water-jacketed CD cell that was kept at 90 ºC. CD spectra were recorded on a Jasco-700 CD spectrometer immediately after liquid, at a predetermined temperature, was flowed from a thermostatting circulating bath through the jacket of the cell. The approximate period required for temperature equilibration after sample transfer was less than 30 seconds since a very small amount of sample was used. The shortest period to complete gelation was 10-15 min. The scan rate and other instrumental parameters were set to optimize the signal-to-noise ratio. Contributions from linear dichroism are negligible since only slight changes in CD intensity were detected when samples were rotated by 90°. Experiments with **CeNC**/ethyl acetate samples were performed in the same way except that the cell was kept at 70 ºC before the hot sols were transferred into the cells.

Kinetics of gelation by fluorescence spectroscopy. **CNC** and *n*-octane were heated until all solids dissolved in a sealed 3 mm pathlength flattened quartz tube (VitroCom). Then,

the tube was placed into a thermostatted cell holder of the fluorimeter (with a VWR-1140 circulating thermostatting bath) and the emission intensity at 375 nm (excitation at 318 nm) was recorded from the front-face as a function of time at a rate of 1 datum per second on Spex Fluorolog III spectrometer. In the data treatment, sets of 10 or 100 consecutive points were averaged and fitted to the kinetic models. The same procedures were employed for preparation of **CeNC**/ethyl acetate samples. The excitation and emission wavelengths were 333 and 358 nm, respectively, and data were recorded on a PTI Qm-Double EX spectrometer equipped with A TLC 50 Fluorescence cuvette holder, a Peltier thermoelectric temperature controller, and Eheim 2028 water circulator.

Kinetics of gelation by small angle neutron scattering (SANS). Data were collected on the 30 m SANS beam line at the National Center for Neutron Research of the National Institute of Standards and Technology, Gaithersburg, MD (5 m scattering, $\lambda = 8.09$ Å) using 2 mm pathlength cylindrical quartz cells placed in a thermostatted (± 0.1 ºC) cell holder. Hot samples of **CNC** with *n*-dodecane-d_{26} as the liquid were transferred to the thermostatted cells as described above. The delay time between the transfer of sample and initial measurements was less than 10 s. In the kinetic runs, intensity data collected in a solid angle defined by a Q range of 0.008-0.1 $Å^{-1}$ were summed during 10 s increments with 35 s delays between collection periods. The sums were plotted then as a function of time to obtain the kinetic parameters as explained in the text. The raw data for the kinetic runs are included in Supporting Table 7.

Kinetics of gelation and thixotropic studies by rheological measurements. Rheology data

were recorded on a Rheometric Scientific RDA-III strain-controlled rheometer using Peltier-controlled parallel plates (25 mm diameter). The sample temperature was controlled to ± 0.1 °C. Experiments were conducted under oscillatory shear, and the storage modulus (*G'*), the loss modulus (*G"*), the ratio between *G"* and *G'* (*tan* δ), and the complex viscosity (η^*) were measured as functions of frequency, ω. The gap between the plates (0.3-0.5 mm) did not influence the rheological data, indicating that wall slip was not a factor.

All rheological experiments were performed with *n*-dodecane, rather than *n*-octane, as the liquid to minimize evaporation from samples at super-ambient temperatures, and at a strain of 1% and a frequency of 10 rad/s, which are within the approximate linear viscoelastic (LVE) regime[4] (Supporting Figure 1); at 40 ºC, slightly below the sol-gel transition temperature, the frequency sweeps indicate that the sample behaves like a soft viscoelastic solid. To reduce evaporation of the solvent further, a plastic cover with a liner soaked with *n*-dodecane was placed over the apparatus when measurements were made at 35 or 40 °C. Hot solutions of **CNC** in *n*-dodecane were transferred onto the lower plate that was at 40 °C when the desired temperature was higher than 20 °C, or at 20 °C higher than the desired temperature when the desired temperature was below 20 °C. The plate was cooled quickly (ca. 30 s) to the desired temperature after the plate gap was adjusted to the desired separation. Recording of kinetic data commenced immediately thereafter.

During rheological measurements to determine thixotropic properties, samples were left undisturbed for 30 min to 4 h (based on the nature of the kinetic study) to complete gelation after the temperature and the gap reached the desired values. The sample was then sheared at a constant shear rate of 2 s^{-1} for 600 s and immediately afterwards, the recovery of *G'* was monitored. A frequency-dependent sweep was also performed both before shearing and after recovery between 0.01-100 rad/s at 1% strain to ascertain whether a 'true' gel was present.[5] After one or two shear-recovery cycles at 25 °C were completed, the plates were separated, a small portion of sample was transferred onto a cover glass with minimal mechanical disturbance using a micro-spatula, and optical micrographs were recorded.

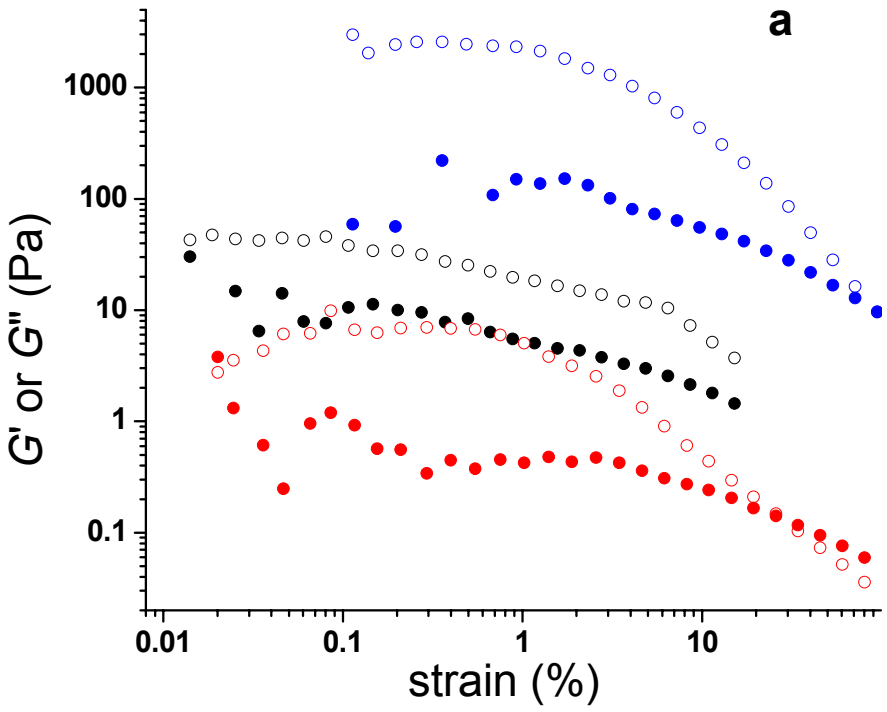
a
1000
100
10
1
0.1
G' or G" (Pa)
0.01
0.1
1
10
strain (%)

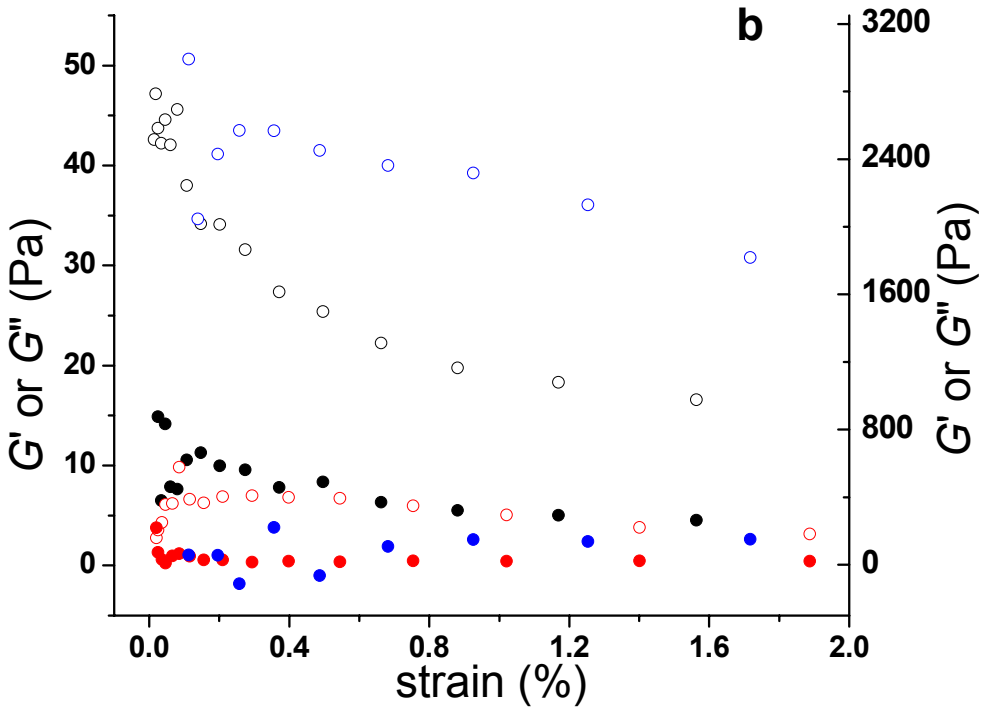
b
50
40
30
20
10
0
G' or G" (Pa)
3200
2400
1600
800
0
G' or G" (Pa)
0.0
0.4
0.8
1.2
1.6
2.0
strain (%)

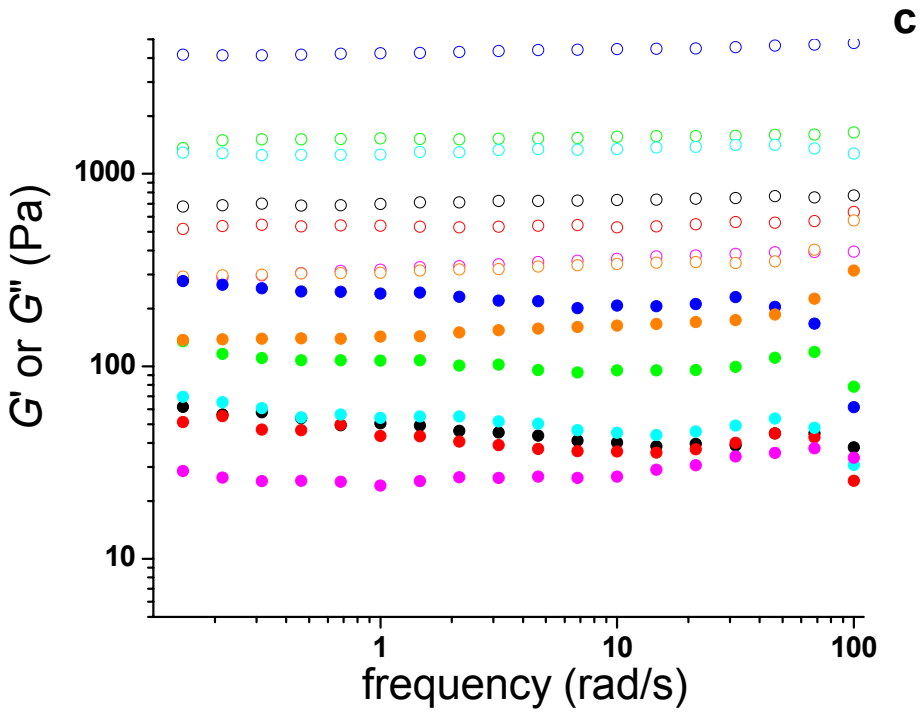

Supporting Figure 1. Log-log (a) and linear (b) strain and frequency (c) sweeps for 1.0 wt% **CNC**/*n*-dodecane gels performed at the temperatures at which the gels were formed (except in the strain sweeps of the gel formed at 40 ºC and measured at 25 ºC (●, ○)). Unfilled symbols are *G'* data; filled symbols are *G"*. (a,b) Gels formed by incubation of sols at 0 (●, ○, left Y-axis) and 40 °C (●, ○, left Y-axis; ●, ○, right Y-axis). (c) Gels formed by incubation of sols at 0 (●, ○), 5 (●, ○), 10 (●, ○), 15 (●, ○), 25 (●, ○), 30 (●, ○) and 40 °C (●, ○).

Supporting Table 2. Gelation studies of **CeNC**[a]

wt%	Liquid	Fast cooling of sol (ice-water bath)	Moderate cooling of sol (in air)	Slow cooling of sol (left in hot water bath that returned slowly to RT)
3	*n*-octane	ppt	ppt	Ppt
3	*n*-decane	PG	PG	PG
3	*n*-dodecane	PG	PG	PG
3	cyclohexane	-	ppt	Ppt

3	$CHCl_3$	Sol	Sol	Sol
3	benzene	-	Sol	Sol
3	toluene	G (< RT)	Sol	Sol
3	CH_3CN	ppt	ppt	Ppt
3	ethyl acetate	G (39.7-46.1)	G (40.2-42.6)	G (43.5-43.7)
2	ethyl acetate	G (40.2-44.7)	G (38.0-40.2)	G (39.9-40.4)
1	ethyl acetate	ppt	ppt	Ppt
0.5	ethyl acetate	Sol	Sol	Sol
0.2	methanol	ppt	ppt	Microcrystal dispersion [b]
0.5	methanol	ppt	ppt	Microcrystal dispersion [b]
1.0	methanol	ppt	ppt	Microcrystal dispersion [b]
1.0	1-propanol	ppt	G (35.1-42.5)	G (44.5-45.0)
1.0	1-butanol	ppt	G (30.0-30.5)	G (30.3-42.9)
1.0	1-pentanol	PG	G (38.0-38.8)	G (38.8-43.0)
1.0	glycerol	ppt	ppt	G (73.5-76.7)
1.0	benzyl alcohol	G (~RT)	G (49.3-55.2)	G (32.0-32.5)
3.0	ethanol	G(86.3-89.1)	G (88.0-90.7)	G (87.2-87.9)
1.0	ethanol	ppt	ppt	Microcrystal dispersion [b]
0.5	ethanol	ppt	Microcrystal dispersion [b]	Microcrystal dispersion [b]
3.0	1-octanol	ppt	G (59.1-71.5)	G (59.9-62.5)
2.0	1-octanol	ppt	G (47.8-56.3)	PG
1.0	1-octanol	some ppt	some ppt	some ppt

[a] G: gel; PG: partial gel; ppt: precipitate; Sol: solution; The values in parentheses are gel-to-sol transition temperatures, T_g, determined by the inverse flow method: sealed tubes with gel samples were inverted and placed next to a thermometer in a water bath at

room temperature and the water bath was stirred and heated. The temperature range for the gel-to-sol transition was taken to be from the moment of initial sample flow to when it fell completely to the bottom of the tube. [b] phase-separated sample of microcrystallites that, when inverted, does not fall.

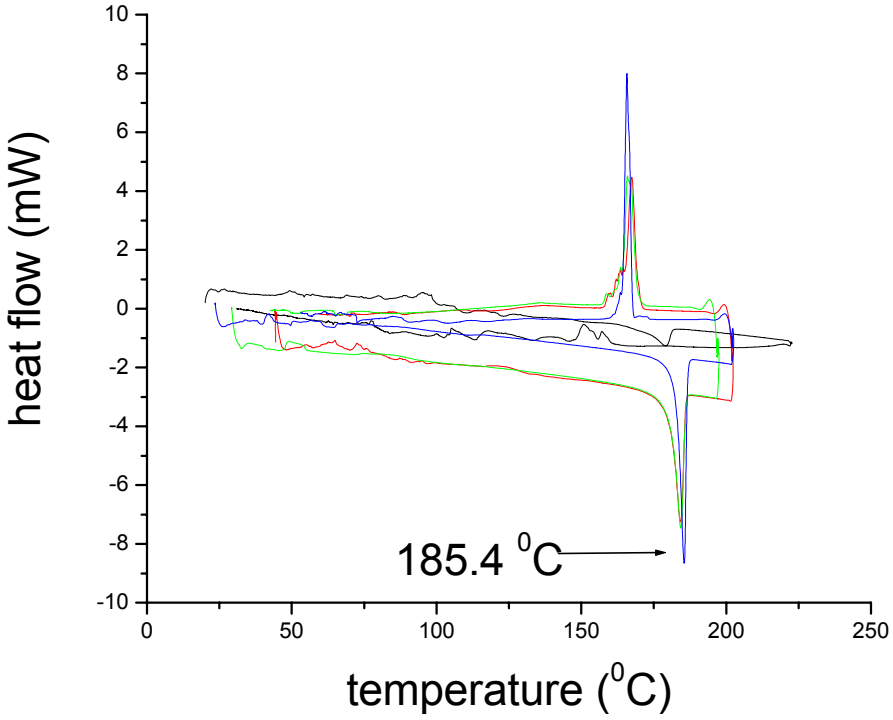

Supporting Figure 2. DSC of **CNC** fiber-like crystal obtained from ethyl acetate (—) and of **CNC** spherulitic solid obtained by drying a MeCN solution (first run, —; second run, —; third run, —).

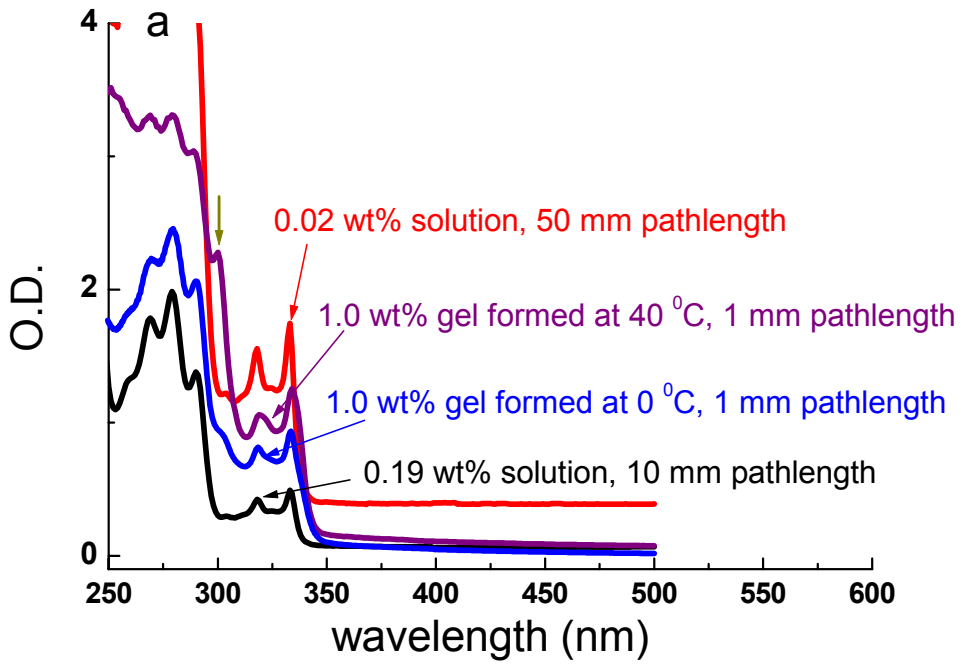
a
4
2
0
O.D.
250
300
350
400
450
500
550
600
wavelength (nm)
0.02 wt% solution, 50 mm pathlength
1.0 wt% gel formed at 40 °C, 1 mm pathlength
1.0 wt% gel formed at 0 °C, 1 mm pathlength
0.19 wt% solution, 10 mm pathlength

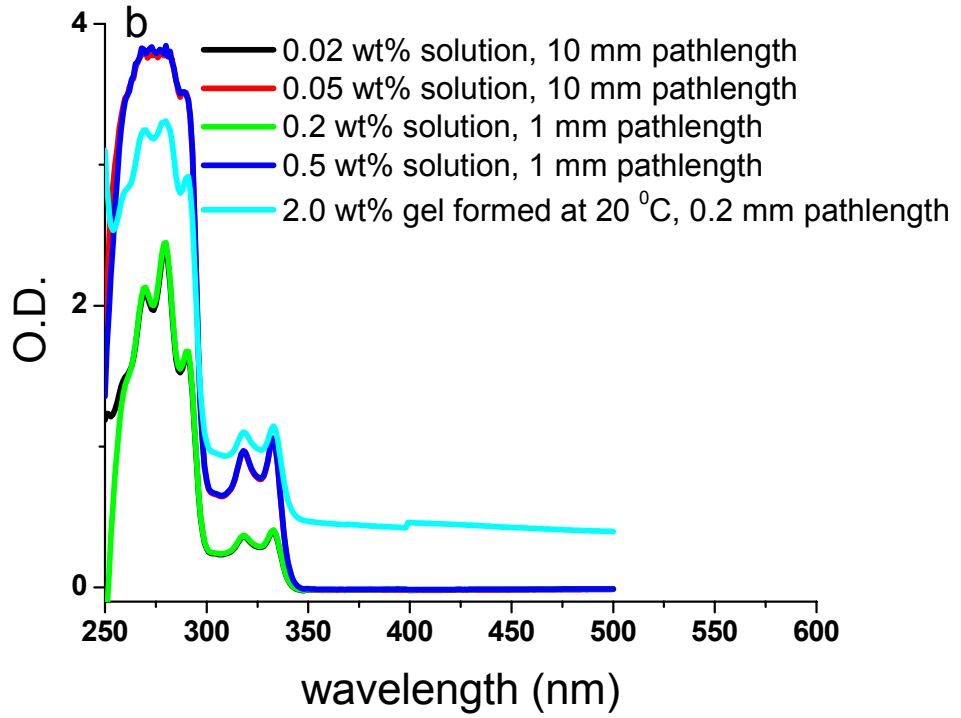
b
4
2
0
O.D.
250
300
350
400
450
500
550
600
wavelength (nm)
0.02 wt% solution, 10 mm pathlength
0.05 wt% solution, 10 mm pathlength
0.2 wt% solution, 1 mm pathlength
0.5 wt% solution, 1 mm pathlength
2.0 wt% gel formed at 20 °C, 0.2 mm pathlength

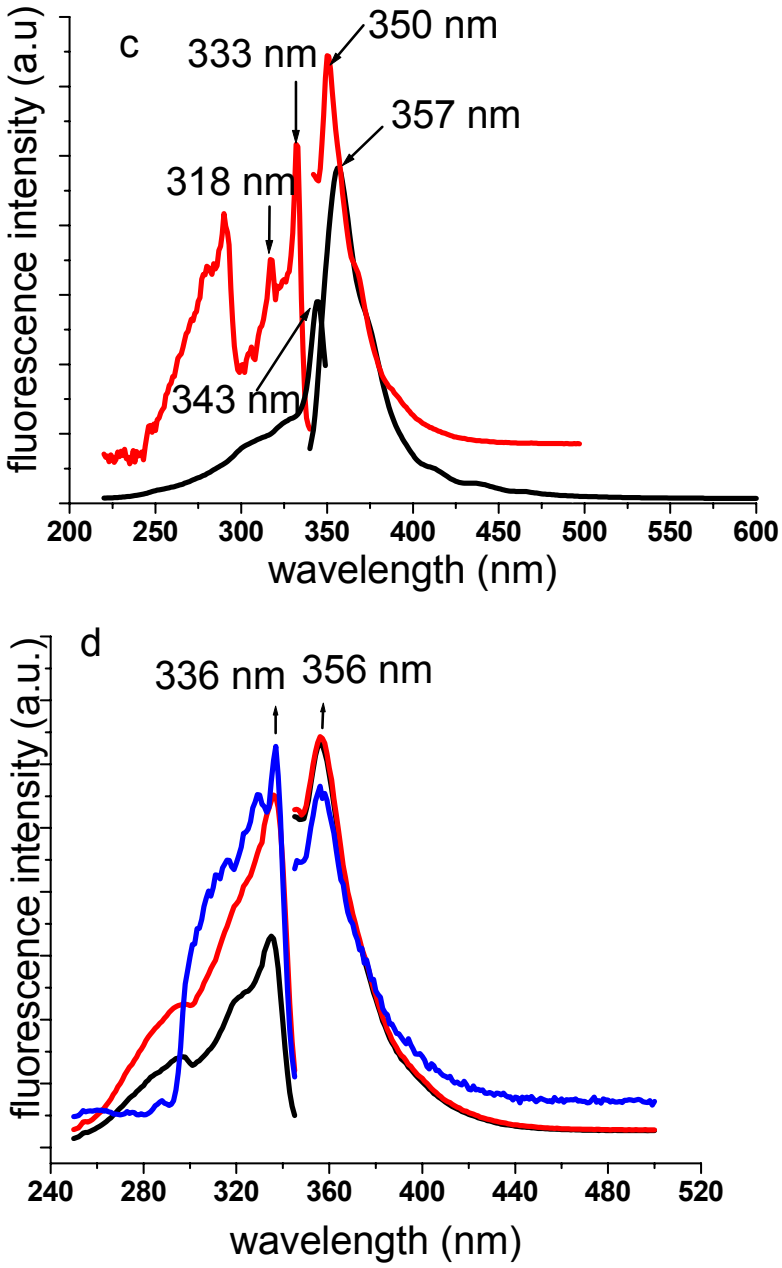

Supporting Figure 3. Absorption spectra at room temperature of a) **CNC** in *n*-octane[6] and b) **CeNC** in ethyl acetate. Data for O.D. values above 3 are inaccurate. c) Emission (right) and excitation (left) spectra of an 0.02 wt% **CNC**/*n*-octane N_2-saturated solution (—, λ_{ex} 318 nm and λ_{em} 350 nm; right-angle geometry) and a 1.0 wt% **CNC**/*n*-octane gel in air formed by incubation of the corresponding sol at 25 °C (—, λ_{ex} 333 nm and λ_{ex} 357

nm; front-face geometry); d) Emission (right) and excitation (left) spectra of 0.01 wt% (—) and 0.5 wt% (—) **CeNC**/ethyl acetate solutions (λ_{ex} 333 nm and λ_{em} 356 nm; right-angle geometry) and a 2.0 wt% **CeNC**/ethyl acetate gel in air formed by incubation of the corresponding sol at 0 °C (—, λ_{ex} 333 nm and λ_{ex} 356 nm; front-face geometry). The wavelengths in the figures are the intensity maxima.

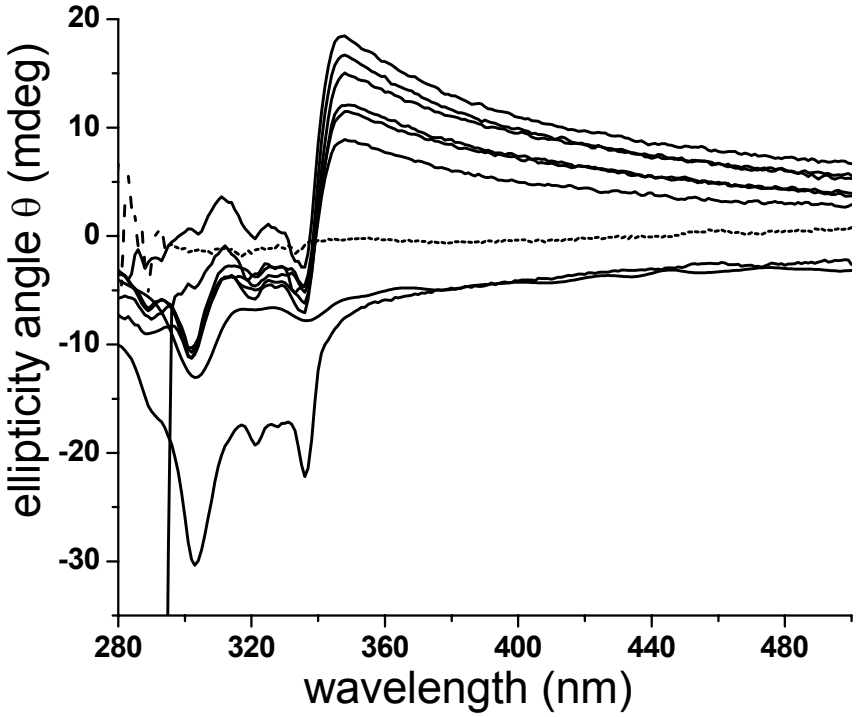

Supporting Figure 4. CD spectra of a 0.02 wt% **CNC**/*n*-octane sol at room temperature (50 mm pathlength cell; dashed line) and 1.0 wt% **CNC**/*n*-octane gels (1mm pathlength cell) formed by cooling the sol rapidly from well above T_g and incubating the sample at 5.4, 8.7, 12.1, 20.2, 25.0, 30.0, 35.0 and 40.0 °C (solid lines, ellipticities from top to bottom at 346 nm).[6]

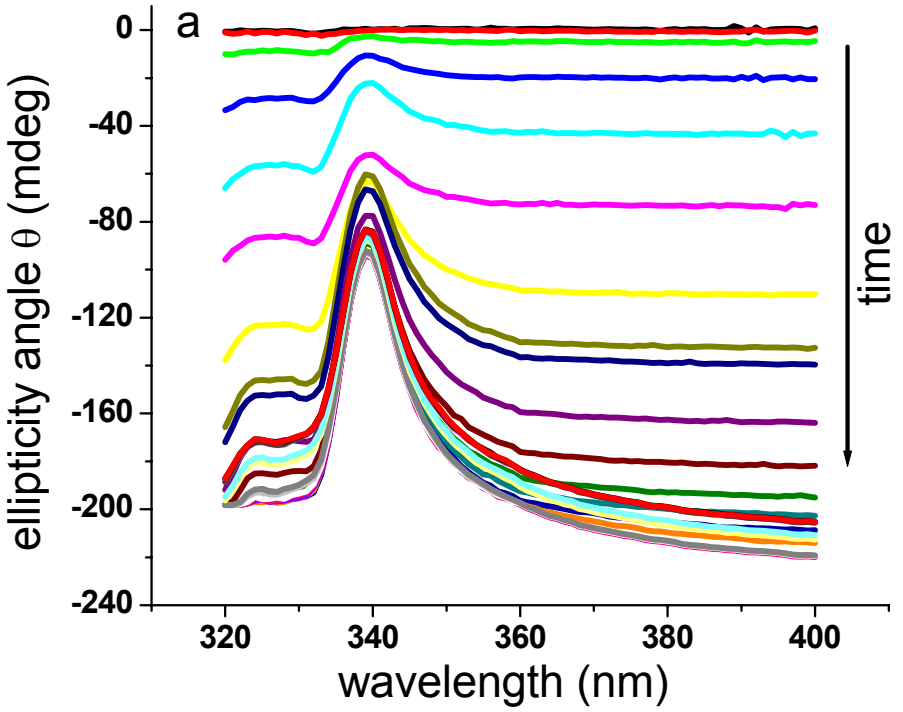
a
0
-40
-80
-120
-160
-200
-240
ellipticity angle θ (mdeg)
320
340
360
380
400
wavelength (nm)
time

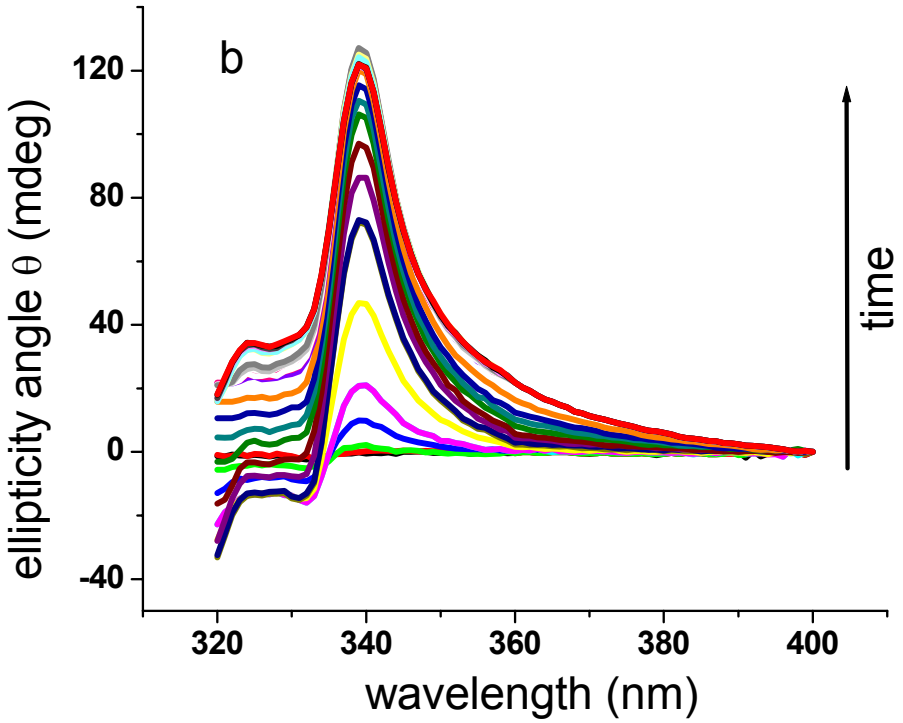
b
120
80
40
0
-40
ellipticity angle θ (mdeg)
320
340
360
380
400
wavelength (nm)
time

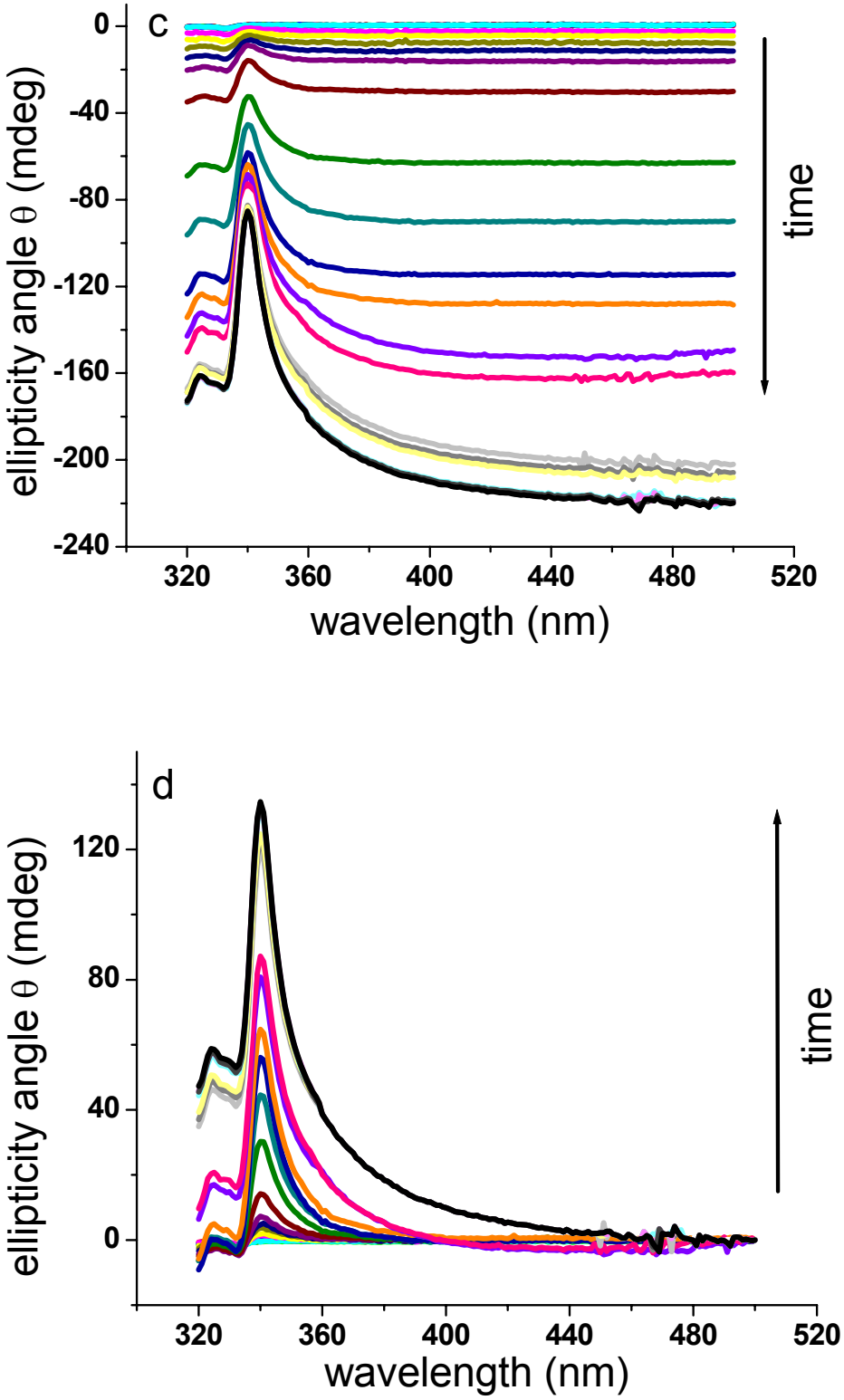

Supporting Figure 5. CD spectra of 2.0 wt% **CeNC**/ethyl acetate hot sols cooled rapidly

to and incubated at 0 in 0.2 mm thick cell (a, b; intervals between the beginning and end of data collection for each sequential spectrum (an accumulation of several scans, each requiring 15 s) were 90, 90, 90, 90, 90, 90, 90, 62, 90, 90, 90, 90, 95, 90, 90, 90, 90, 241, 150, 995, 150, 1954, 150, and 1558 s; the total time was 6742.5 s) or at 20 °C (c, d; intervals between the beginning and end of data collection for each sequential spectrum (an accumulation of several scans, each requiring 55 s) were 825, 3050.5, 550, 550, 1962, 330, 330, 330, 330, 503, 1174, 1003, 1003, 330, 330, 330, 330, 1187, 550, 550, 2424, 550, 550, and 986 s; the total time is 20342.5 s) to follow gel formation. In (b) and (d), the spectra have been offset to normalize ellipticities to 0 degrees at 400 (b) or 500 nm (d).

Supporting Table 3. Summary of fractal dimensions of SAFINs from 1.0 wt% **CNC**/*n*-alkane gels formed by incubation of sols at different temperatures using data from different techniques.

Temp (± 0.1˚C)	D_f (from fluorescence)	R^2
1.1	1.74	0.993
3.8	1.72	0.993
9.3	1.75	0.992
13.9	1.70	0.994
22.5	1.79	0.991
23.8	1.80	0.992
32.0	1.42	0.983
32.2	1.38	0.992
39.2	1.38	0.988
	(from SANS)	
40.0	1.38	0.997
	(from CD)	
5.0	1.72	0.989
8.0	1.73	0.985
12.0	1.68	0.989
16.0	1.71	0.991
20.0	1.75	0.976
25.0	1.64	0.996
30.0	1.37	0.993
40.0	1.35 (304 nm)	0.982
	1.42 (336 nm)	0.992

	(from rheology)	
0.0	1.78	0.998
5.0	1.70	0.996
10.0	1.75	0.991
15.0	1.73	0.991
30.0	1.36	0.991
35.0	1.38	0.998
40.0	1.38	0.998

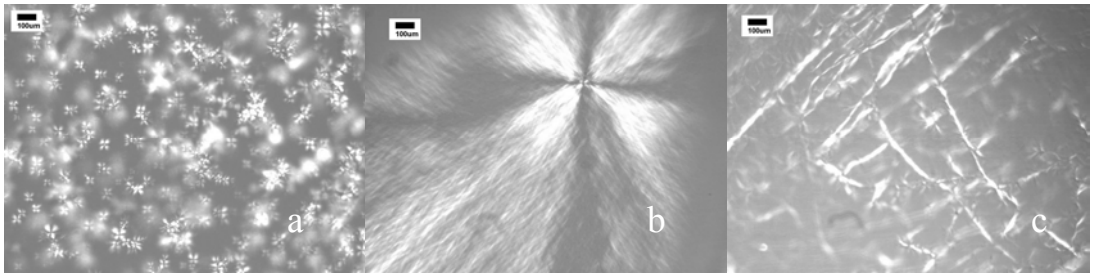

Supporting Figure 6. Optical micrographs of 1.0 wt% **CNC**/*n*-octane gels formed at 0, 25.1 and 37.4 °C.[6] Scale bars = 100 μm.

Supporting Table 4. Summary of fractal dimensions of SAFINs in gels from incubation of sols at 32.2 °C with different concentrations of **CNC**/*n*-octane using data from fluorescence.		
[**CNC**] (wt%)	D_f	R^2
3.0	1.76	0.981
2.5	1.73	0.992
1.94	1.72	0.991
1.46	1.69	0.991
1.0	1.38	0.992
0.89	1.32	0.993

Supporting Table 5. Summary of fractal dimensions and Avrami parameters for 2.0 wt% **CeNC**/ethyl acetate gels formed by incubation of sols at various temperatures from data using different techniques.					
Temperature (± 0.1˚C)	*n*	K (s^{-1})	R^2	D_f	R^2
(from fluorescence)					
21.9	2.05	-15.3	0.995	1.15	0.994

20.5	2.07	-15.0	0.996	1.14	0.995
20.4	1.92	-18.6	0.999	1.14	0.999
16.1	2.06	-13.0	0.994	1.14	0.988
12.0	1.99	-13.7	0.994	1.30	0.988
11.4	2.12	-15.3	0.994	1.15	0.997
8.2	2.00	-11.4	0.995	1.29	0.986
7.0	2.08	-15.1	0.997	1.12	0.995
3.4	2.07	-12.2	0.995	1.16	0.997
2.5	1.73	-12.2	0.993	1.24	0.998
0.3	1.07	-6.45	0.996	1.30	0.996
-2.6	1.12	-5.55	0.995	1.29	0.988
-4.1	1.17	-6.87	0.991	1.29	0.986
-7.3	1.05	-8.00	0.993	1.30	0.999
-8.4	1.06	-6.33	0.992	1.27	0.992
(from CD)					
20.2	2.09	-18.2	0.990	1.11	0.992
0.6	1.89	-12.2	0.993	1.23	0.986

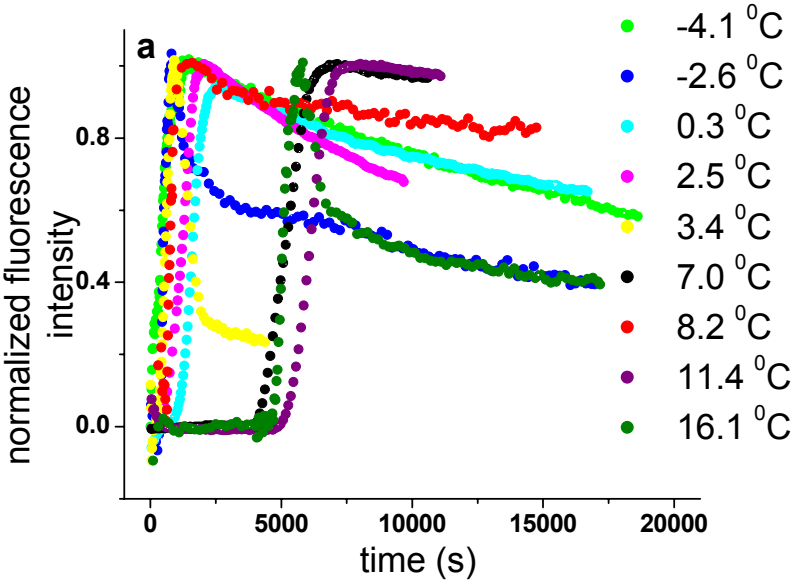
a
normalized fluorescence intensity
0.0
0.4
0.8
0
5000
10000
15000
20000
time (s)
-4.1 °C
-2.6 °C
0.3 °C
2.5 °C
3.4 °C
7.0 °C
8.2 °C
11.4 °C
16.1 °C

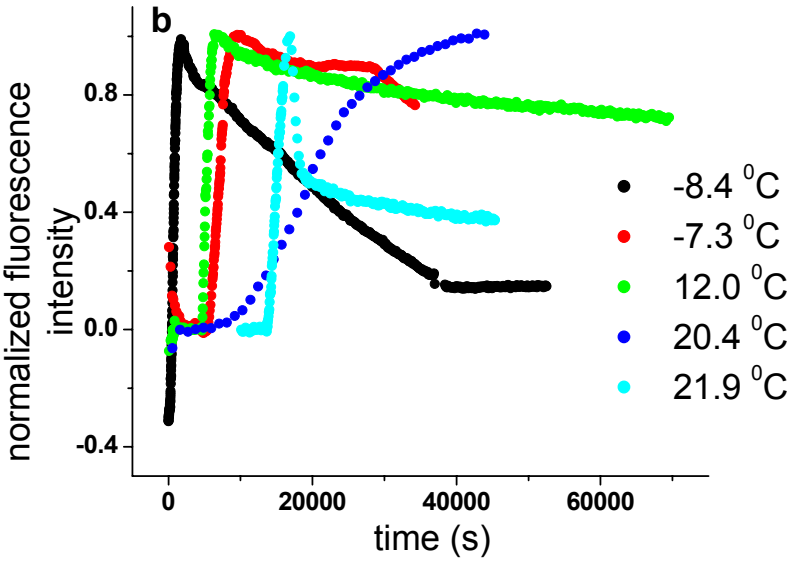
b
normalized fluorescence intensity
-0.4
0.0
0.4
0.8
0
20000
40000
60000
time (s)
-8.4 °C
-7.3 °C
12.0 °C
20.4 °C
21.9 °C

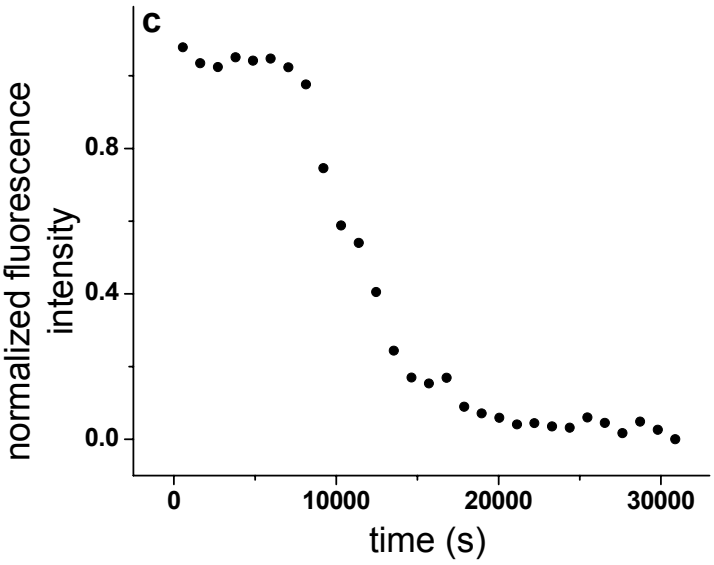

Supporting Figure 7. Normalized fluorescence intensity (λ_{em} 358 nm; λ_{ex} 333 nm) changes versus time for sols cooled rapidly to and incubated at the temperatures indicated in (a, b) 2.0 wt% **CeNC**/ethyl acetate or at 24.9 °C in (c) 2.0 wt% **CeNC**/ethyl acetate where crystallization and macroscopic phase separation occurred.

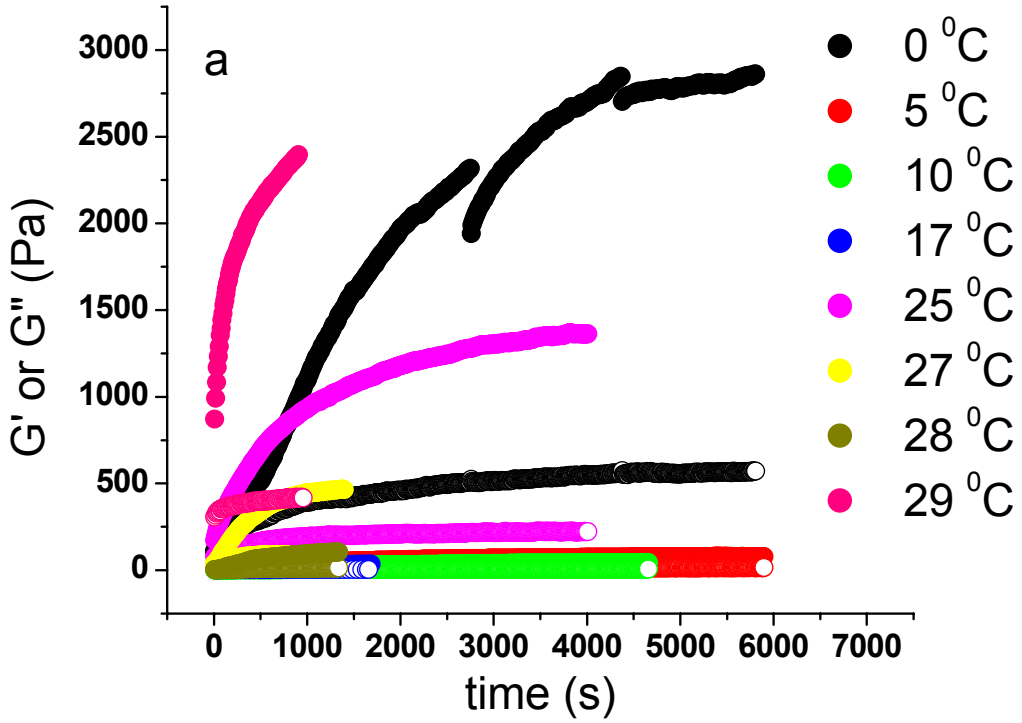

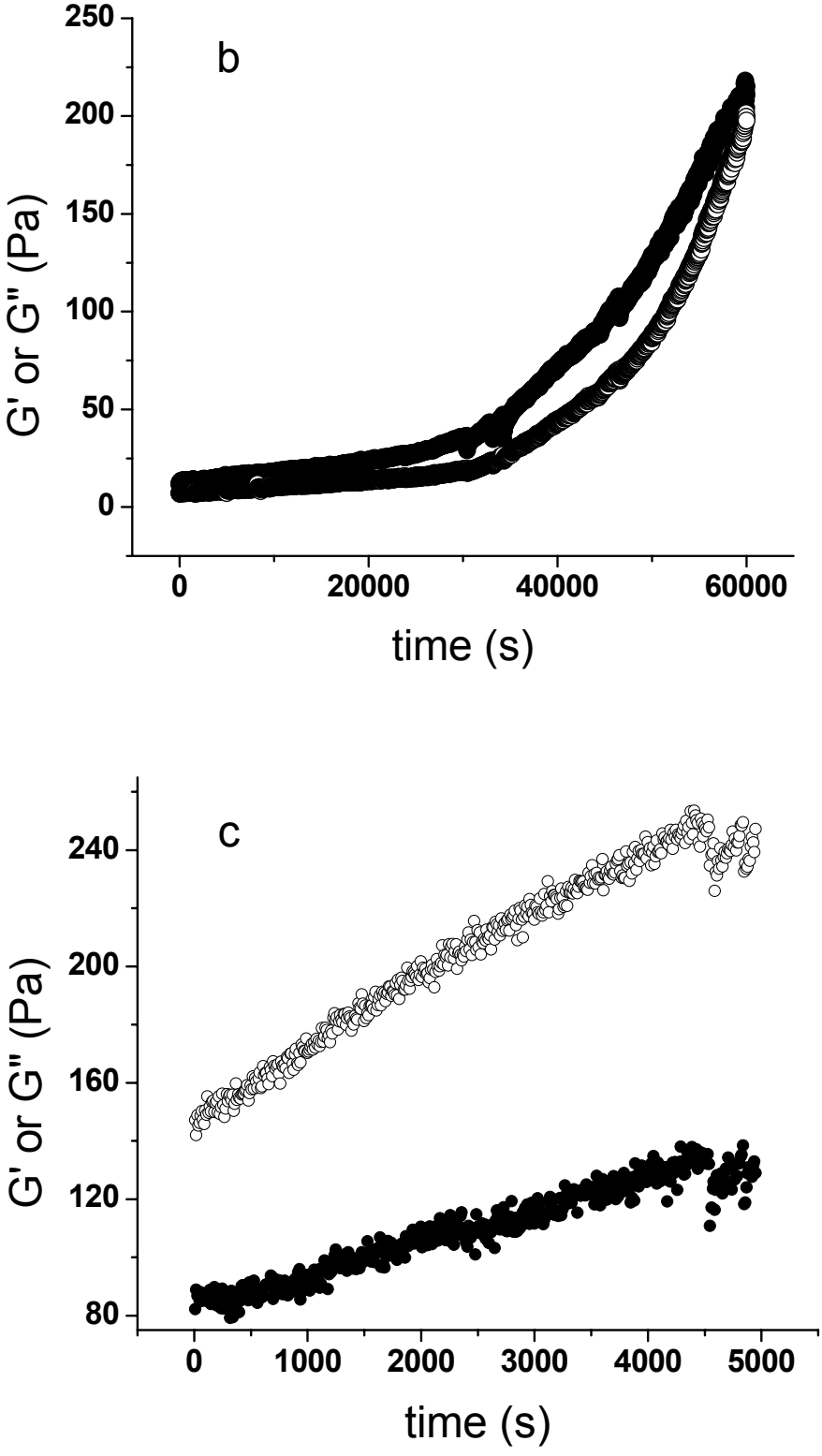

Supporting Figure 8. Recovery of viscoelastic properties of 1.0 wt% **CNC**/*n*-dodecane

gels (formed by incubation of the sols at 30 and 40 °C, respectively) after being sheared at 2 rad/s for 600 s and left at the temperatures shown in a). In b) (30 °C) and c) (40 °C), *G'* is filled symbols and *G"* is open symbols.

Supporting Table 6. Summary of τ values from single exponential fits of individual *G'* and *G"* values of 1.0 wt% **CNC**/*n*-dodecane gels formed by incubation of the sols at the temperatures indicated and then sheared at 2 rad/s for 600 s at the same temperatures.

Temperature (± 0.1 °C)	from *G'* ($\times 10^2$ s)	from *G"* ($\times 10^2$ s)
0.0	15.3±0.2	14.7±0.2
5.0	16.0±0.1	17.9±0.2
10.0	29.0±0.2	29.0±0.3
10.0	13. 5±0.3	13.4±0.3
17.0	8.39±0.24	6.03±0.29
25.0	8.67±0.17	6.68±0.46
25.0	11.1±0.2	5.81±0.18
27.0	4.22±0.03	1.94±0. 05
27.0	4.76±0.12	1.84±0.08
27.0	5.34±0.13	1.85±0.04
28.0	4.29±0.05	4.12±0.06
28.0	3.89±0.07	4.02±0.11
29.0	3.05±0.04	3.15±0.07

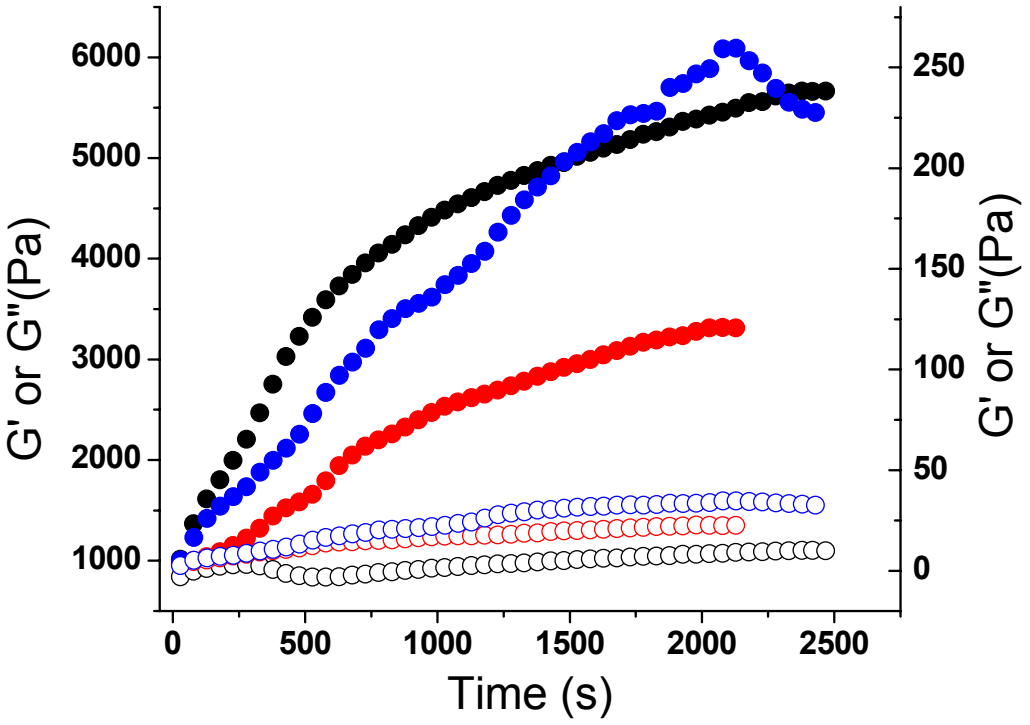

Supporting Figure 9. Recovery of *G'* (filled symbols) and *G"* (open symbols) of 3.0 wt% **CNC**/*n*-dodecane gels (formed by incubation of the sols at 0, 15 or 30 °C) after being sheared at 2 rad/s for 600 s at 0 (○, ●; left axis), 15 (○, ●; right axis) and 30 °C (○, ●; right axis).

Supporting Table 7. SANS data for kinetic runs. Summed counts during 10 s intervals with 35 s dead time between intervals.

File names	Labels	Date and time	Tot. cnts
OCT03207.SA2_RW_E916	5M Scatt KIN2 CNC 3% 40c	10/17/2003 9:30	18
OCT03208.SA2_RW_E917	5M Scatt KIN2 CNC 3% 40c	10/17/2003 9:40	1142
OCT03209.SA2_RW_E918	5M Scatt KIN2 CNC 3% 40c	10/17/2003 9:41	1067
OCT03210.SA2_RW_E919	5M Scatt KIN2 CNC 3% 40c	10/17/2003 9:42	3594
OCT03211.SA2_RW_E920	5M Scatt KIN2 CNC 3% 40c	10/17/2003 9:43	54922
OCT03212.SA2_RW_E921	5M Scatt KIN2 CNC 3% 40c	10/17/2003 9:44	81967
OCT03213.SA2_RW_E922	5M Scatt KIN2 CNC 3% 40c	10/17/2003 9:44	87096
OCT03214.SA2_RW_E923	5M Scatt KIN2 CNC 3% 40c	10/17/2003 9:45	89598
OCT03215.SA2_RW_E924	5M Scatt KIN2 CNC 3% 40c	10/17/2003 9:46	90928
OCT03216.SA2_RW_E925	5M Scatt KIN2 CNC 3% 40c	10/17/2003 9:47	92230
OCT03217.SA2_RW_E926	5M Scatt KIN2 CNC 3% 40c	10/17/2003 9:47	92830
OCT03218.SA2_RW_E927	5M Scatt KIN2 CNC 3% 40c	10/17/2003 9:48	93297
OCT03219.SA2_RW_E928	5M Scatt KIN2 CNC 3% 40c	10/17/2003 9:49	93350
OCT03220.SA2_RW_E929	5M Scatt KIN2 CNC 3% 40c	10/17/2003 9:50	93905
OCT03221.SA2_RW_E930	5M Scatt KIN2 CNC 3% 40c	10/17/2003 9:51	94184
OCT03222.SA2_RW_E931	5M Scatt KIN2 CNC 3% 40c	10/17/2003 9:51	93876
OCT03223.SA2_RW_E932	5M Scatt KIN2 CNC 3% 40c	10/17/2003 9:52	94709
OCT03224.SA2_RW_E933	5M Scatt KIN2 CNC 3% 40c	10/17/2003 9:53	94879
OCT03225.SA2_RW_E934	5M Scatt KIN2 CNC 3% 40c	10/17/2003 9:54	93817
OCT03226.SA2_RW_E935	5M Scatt KIN2 CNC 3% 40c	10/17/2003 9:54	94059
OCT03227.SA2_RW_E936	5M Scatt KIN2 CNC 3% 40c	10/17/2003 9:55	94643
OCT03228.SA2_RW_E937	5M Scatt KIN2 CNC 3% 40c	10/17/2003 9:56	94552
OCT03229.SA2_RW_E938	5M Scatt KIN2 CNC 3% 40c	10/17/2003 9:57	95486
OCT03230.SA2_RW_E939	5M Scatt KIN2 CNC 3% 40c	10/17/2003 9:58	94875
OCT03231.SA2_RW_E940	5M Scatt KIN2 CNC 3% 40c	10/17/2003 9:58	94638
OCT03232.SA2_RW_E941	5M Scatt KIN2 CNC 3% 40c	10/17/2003 9:59	94142
OCT03233.SA2_RW_E942	5M Scatt KIN2 CNC 3% 40c	10/17/2003 10:00	94764
OCT03234.SA2_RW_E943	5M Scatt KIN2 CNC 3% 40c	10/17/2003 10:08	94645
OCT03235.SA2_RW_E944	5M Scatt KIN2 CNC 3% 40c	10/17/2003 10:09	94597
OCT03236.SA2_RW_E945	5M Scatt KIN2 CNC 3% 40c	10/17/2003 10:10	95577
OCT03237.SA2_RW_E946	5M Scatt KIN2 CNC 3% 40c	10/17/2003 10:11	95381
OCT03238.SA2_RW_E947	5M Scatt KIN2 CNC 3% 40c	10/17/2003 10:11	94927
OCT03239.SA2_RW_E948	5M Scatt KIN2 CNC 3% 40c	10/17/2003 10:12	95178
OCT03240.SA2_RW_E949	5M Scatt KIN2 CNC 3% 40c	10/17/2003 10:13	95102
OCT03241.SA2_RW_E950	5M Scatt KIN2 CNC 3% 40c	10/17/2003 10:14	95296
OCT03242.SA2_RW_E951	5M Scatt KIN2 CNC 3% 40c	10/17/2003 10:14	94915
OCT03243.SA2_RW_E952	5M Scatt KIN2 CNC 3% 40c	10/17/2003 10:15	94590

OCT03244.SA2_RW_E953	5M Scatt KIN2 CNC 3% 40c	10/17/2003 10:16	95307
OCT03245.SA2_RW_E954	5M Scatt KIN2 CNC 3% 40c	10/17/2003 10:29	95355
OCT03246.SA2_RW_E955	5M Scatt KIN2 CNC 3% 40c	10/17/2003 10:30	95374
OCT03247.SA2_RW_E956	5M Scatt KIN2 CNC 3% 40c	10/17/2003 10:30	95383
OCT03248.SA2_RW_E957	5M Scatt KIN2 CNC 3% 40c	10/17/2003 10:31	95419
OCT03249.SA2_RW_E958	5M Scatt KIN2 CNC 3% 40c	10/17/2003 10:32	95381
OCT03250.SA2_RW_E959	5M Scatt KIN2 CNC 3% 40c	10/17/2003 10:33	95618
OCT03251.SA2_RW_E960	5M Scatt KIN2 CNC 3% 40c	10/17/2003 10:47	95742
OCT03252.SA2_RW_E961	5M Scatt KIN2 CNC 3% 40c	10/17/2003 10:47	96035
OCT03253.SA2_RW_E962	5M Scatt KIN2 CNC 3% 40c	10/17/2003 10:48	95971
OCT03254.SA2_RW_E963	5M Scatt KIN2 CNC 3% 40c	10/17/2003 10:49	96575
OCT03255.SA2_RW_E964	5M Scatt KIN2 CNC 3% 40c	10/17/2003 10:50	95293
OCT03256.SA2_RW_E965	5M Scatt KIN2 CNC 3% 40c	10/17/2003 10:50	95791
OCT03257.SA2_RW_E966	5M Scatt KIN2 CNC 3% 40c	10/17/2003 10:59	1091
OCT03258.SA2_RW_E967	5M Scatt KIN2 CNC 3% 40c	10/17/2003 11:00	1059
OCT03259.SA2_RW_E968	5M Scatt KIN2 CNC 3% 40c	10/17/2003 11:01	1138
OCT03260.SA2_RW_E969	5M Scatt KIN2 CNC 3% 40c	10/17/2003 11:01	7163
OCT03261.SA2_RW_E970	5M Scatt KIN2 CNC 3% 40c	10/17/2003 11:02	65098
OCT03262.SA2_RW_E971	5M Scatt KIN2 CNC 3% 40c	10/17/2003 11:03	81951
OCT03263.SA2_RW_E972	5M Scatt KIN2 CNC 3% 40c	10/17/2003 11:04	85692
OCT03264.SA2_RW_E973	5M Scatt KIN2 CNC 3% 40c	10/17/2003 11:04	89038
OCT03265.SA2_RW_E974	5M Scatt KIN2 CNC 3% 40c	10/17/2003 11:05	90151
OCT03266.SA2_RW_E975	5M Scatt KIN2 CNC 3% 40c	10/17/2003 11:06	91426
OCT03267.SA2_RW_E976	5M Scatt KIN2 CNC 3% 40c	10/17/2003 11:07	92312
OCT03268.SA2_RW_E977	5M Scatt KIN2 CNC 3% 40c	10/17/2003 11:08	92837
OCT03269.SA2_RW_E978	5M Scatt KIN2 CNC 3% 40c	10/17/2003 11:08	93219
OCT03270.SA2_RW_E979	5M Scatt KIN2 CNC 3% 40c	10/17/2003 11:09	93049
OCT03271.SA2_RW_E980	5M Scatt KIN2 CNC 3% 40c	10/17/2003 11:10	93263
OCT03272.SA2_RW_E981	5M Scatt KIN2 CNC 3% 40c	10/17/2003 11:11	93387
OCT03273.SA2_RW_E982	5M Scatt KIN2 CNC 3% 40c	10/17/2003 11:11	93566
OCT03274.SA2_RW_E983	5M Scatt KIN2 CNC 3% 40c	10/17/2003 11:12	94525
OCT03275.SA2_RW_E984	5M Scatt KIN2 CNC 3% 40c	10/17/2003 11:13	94292
OCT03276.SA2_RW_E985	5M Scatt KIN2 CNC 3% 40c	10/17/2003 11:14	94593
OCT03277.SA2_RW_E986	5M Scatt KIN2 CNC 3% 40c	10/17/2003 11:14	94291
OCT03278.SA2_RW_E987	5M Scatt KIN2 CNC 3% 40c	10/17/2003 11:15	94602
OCT03279.SA2_RW_E988	5M Scatt KIN2 CNC 3% 40c	10/17/2003 11:16	94953
OCT03280.SA2_RW_E989	5M Scatt KIN2 CNC 3% 40c	10/17/2003 11:17	94475
OCT03281.SA2_RW_E990	5M Scatt KIN2 CNC 3% 40c	10/17/2003 11:18	94224
OCT03282.SA2_RW_E991	5M Scatt KIN2 CNC 3% 40c	10/17/2003 11:18	95089
OCT03283.SA2_RW_E992	5M Scatt KIN2 CNC 3% 40c	10/17/2003 11:30	95052
OCT03284.SA2_RW_E993	5M Scatt KIN2 CNC 3% 40c	10/17/2003 11:30	95641

OCT03285.SA2_RW_E994	5M Scatt KIN2 CNC 3% 40c	10/17/2003 11:31	95458
OCT03286.SA2_RW_E995	5M Scatt KIN2 CNC 3% 40c	10/17/2003 11:32	95800
OCT03287.SA2_RW_E996	5M Scatt KIN2 CNC 3% 40c	10/17/2003 11:33	96311
OCT03288.SA2_RW_E997	5M Scatt KIN2 CNC 3% 40c	10/17/2003 11:33	95669
OCT03289.SA2_RW_E998	5M Scatt KIN2 CNC 3% 40c	10/17/2003 11:34	95505
OCT03290.SA2_RW_E999	5M Scatt KIN2 CNC 3% 40c	10/17/2003 11:35	95654
OCT03291.SA2_RW_F000	5M Scatt KIN2 CNC 3% 40c	10/17/2003 11:36	96321
OCT03292.SA2_RW_F001	5M Scatt KIN2 CNC 3% 40c	10/17/2003 11:36	96215
OCT03293.SA2_RW_F002	5M Scatt KIN2 CNC 3% 40c	10/17/2003 11:37	96221
OCT03294.SA2_RW_F003	5M Scatt KIN2 CNC 3% 40c	10/17/2003 12:10	96760
OCT03295.SA2_RW_F004	5M Scatt KIN2 CNC 3% 40c	10/17/2003 12:11	97056
OCT03296.SA2_RW_F005	5M Scatt KIN2 CNC 3% 40c	10/17/2003 12:11	96447
OCT03297.SA2_RW_F006	5M Scatt KIN2 CNC 3% 40c	10/17/2003 12:12	96861
OCT03298.SA2_RW_F007	5M Scatt KIN2 CNC 3% 40c	10/17/2003 12:13	97412
OCT03299.SA2_RW_F008	5M Scatt KIN2 CNC 3% 40c	10/17/2003 12:14	97315
OCT03300.SA2_RW_F009	5M Scatt KIN2 CNC 3% 40c	10/17/2003 12:14	97273
OCT03301.SA2_RW_F010	5M Scatt KIN2 CNC 3% 40c	10/17/2003 12:15	96928
OCT03302.SA2_RW_F011	5M Scatt KIN2 CNC 3% 40c	10/17/2003 12:16	95793
OCT03303.SA2_RW_F012	5M Scatt KIN2 CNC 3% 40c	10/17/2003 12:17	96279
OCT03304.SA2_RW_F013	5M Scatt KIN2 CNC 3% 40c	10/17/2003 12:17	97164
OCT03305.SA2_RW_F014	5M Scatt KIN2 CNC 3% 40c	10/17/2003 12:28	97245
OCT03306.SA2_RW_F015	5M Scatt KIN2 CNC 3% 40c	10/17/2003 12:28	96820
OCT03307.SA2_RW_F016	5M Scatt KIN2 CNC 3% 40c	10/17/2003 12:29	97463
OCT03308.SA2_RW_F017	5M Scatt KIN2 CNC 3% 40c	10/17/2003 12:30	97556
OCT03309.SA2_RW_F018	5M Scatt KIN2 CNC 3% 40c	10/17/2003 12:31	97627
OCT03310.SA2_RW_F019	5M Scatt KIN2 CNC 3% 40c	10/17/2003 12:31	97709
OCT03311.SA2_RW_F020	5M Scatt KIN2 CNC 3% 40c	10/17/2003 12:32	96580
OCT03312.SA2_RW_F021	5M Scatt KIN2 CNC 3% 40c	10/17/2003 12:33	96952
OCT03313.SA2_RW_F022	5M Scatt KIN2 CNC 3% 40c	10/17/2003 12:34	97308
OCT03314.SA2_RW_F023	5M Scatt KIN2 CNC 3% 40c	10/17/2003 12:34	97114
OCT03315.SA2_RW_F024	5M Scatt KIN2 CNC 3% 40c	10/17/2003 12:35	97538
OCT03316.SA2_RW_F025	5M Scatt KIN2 CNC 3% 40c	10/17/2003 12:42	97689
OCT03317.SA2_RW_F026	5M Scatt KIN2 CNC 3% 40c	10/17/2003 12:43	97592
OCT03318.SA2_RW_F027	5M Scatt KIN2 CNC 3% 40c	10/17/2003 12:44	97497
OCT03319.SA2_RW_F028	5M Scatt KIN2 CNC 3% 40c	10/17/2003 12:45	97200
OCT03320.SA2_RW_F029	5M Scatt KIN2 CNC 3% 40c	10/17/2003 12:46	97189
OCT03321.SA2_RW_F030	5M Scatt KIN2 CNC 3% 40c	10/17/2003 12:46	98019
OCT03322.SA2_RW_F031	5M Scatt KIN CNC 1% 40c	10/17/2003 12:55	856
OCT03323.SA2_RW_F032	5M Scatt KIN CNC 1% 40c	10/17/2003 12:55	899
OCT03324.SA2_RW_F033	5M Scatt KIN CNC 1% 40c	10/17/2003 12:56	893
OCT03325.SA2_RW_F034	5M Scatt KIN CNC 1% 40c	10/17/2003 12:57	867

OCT03326.SA2_RW_F035	5M Scatt KIN CNC 1% 40c	10/17/2003 12:58	944
OCT03327.SA2_RW_F036	5M Scatt KIN CNC 1% 40c	10/17/2003 12:59	897
OCT03328.SA2_RW_F037	5M Scatt KIN CNC 1% 40c	10/17/2003 12:59	883
OCT03329.SA2_RW_F038	5M Scatt KIN CNC 1% 40c	10/17/2003 13:00	882
OCT03330.SA2_RW_F039	5M Scatt KIN CNC 1% 40c	10/17/2003 13:01	874
OCT03331.SA2_RW_F040	5M Scatt KIN CNC 1% 40c	10/17/2003 13:02	920
OCT03332.SA2_RW_F041	5M Scatt KIN CNC 1% 40c	10/17/2003 13:02	941
OCT03333.SA2_RW_F042	5M Scatt KIN CNC 1% 40c	10/17/2003 13:08	1290
OCT03334.SA2_RW_F043	5M Scatt KIN CNC 1% 40c	10/17/2003 13:09	1306
OCT03335.SA2_RW_F044	5M Scatt KIN CNC 1% 40c	10/17/2003 13:10	1340
OCT03336.SA2_RW_F045	5M Scatt KIN CNC 1% 40c	10/17/2003 13:11	1370
OCT03337.SA2_RW_F046	5M Scatt KIN CNC 1% 40c	10/17/2003 13:11	1471
OCT03338.SA2_RW_F047	5M Scatt KIN CNC 1% 40c	10/17/2003 13:12	1578
OCT03339.SA2_RW_F048	5M Scatt KIN CNC 1% 40c	10/17/2003 13:21	2145
OCT03340.SA2_RW_F049	5M Scatt KIN CNC 1% 40c	10/17/2003 13:21	2227
OCT03341.SA2_RW_F050	5M Scatt KIN CNC 1% 40c	10/17/2003 13:22	2399
OCT03342.SA2_RW_F051	5M Scatt KIN CNC 1% 40c	10/17/2003 13:23	2375
OCT03343.SA2_RW_F052	5M Scatt KIN CNC 1% 40c	10/17/2003 13:24	2446
OCT03344.SA2_RW_F053	5M Scatt KIN CNC 1% 40c	10/17/2003 13:24	2569
OCT03345.SA2_RW_F054	5M Scatt KIN CNC 1% 40c	10/17/2003 13:25	2655
OCT03346.SA2_RW_F055	5M Scatt KIN CNC 1% 40c	10/17/2003 13:26	2702
OCT03347.SA2_RW_F056	5M Scatt KIN CNC 1% 40c	10/17/2003 13:27	2767
OCT03348.SA2_RW_F057	5M Scatt KIN CNC 1% 40c	10/17/2003 13:27	2904
OCT03349.SA2_RW_F058	5M Scatt KIN CNC 1% 40c	10/17/2003 13:28	2909
OCT03350.SA2_RW_F059	5M Scatt KIN CNC 1% 40c	10/17/2003 13:33	3496
OCT03351.SA2_RW_F060	5M Scatt KIN CNC 1% 40c	10/17/2003 13:34	3530
OCT03352.SA2_RW_F061	5M Scatt KIN CNC 1% 40c	10/17/2003 13:35	3549
OCT03353.SA2_RW_F062	5M Scatt KIN CNC 1% 40c	10/17/2003 13:35	3539
OCT03354.SA2_RW_F063	5M Scatt KIN CNC 1% 40c	10/17/2003 13:36	3682
OCT03355.SA2_RW_F064	5M Scatt KIN CNC 1% 40c	10/17/2003 13:37	3769
OCT03356.SA2_RW_F065	5M Scatt KIN CNC 1% 40c	10/17/2003 13:38	3884
OCT03357.SA2_RW_F066	5M Scatt KIN CNC 1% 40c	10/17/2003 13:38	4054
OCT03358.SA2_RW_F067	5M Scatt KIN CNC 1% 40c	10/17/2003 13:39	4021
OCT03359.SA2_RW_F068	5M Scatt KIN CNC 1% 40c	10/17/2003 13:40	4089
OCT03360.SA2_RW_F069	5M Scatt KIN CNC 1% 40c	10/17/2003 13:41	4230
OCT03361.SA2_RW_F070	5M Scatt KIN CNC 1% 40c	10/17/2003 13:42	4165
OCT03362.SA2_RW_F071	5M Scatt KIN CNC 1% 40c	10/17/2003 13:42	4346
OCT03363.SA2_RW_F072	5M Scatt KIN CNC 1% 40c	10/17/2003 13:43	4399
OCT03364.SA2_RW_F073	5M Scatt KIN CNC 1% 40c	10/17/2003 13:44	4452
OCT03365.SA2_RW_F074	5M Scatt KIN CNC 1% 40c	10/17/2003 13:45	4603
OCT03366.SA2_RW_F075	5M Scatt KIN CNC 1% 40c	10/17/2003 13:45	4693

OCT03367.SA2_RW_F076	5M Scatt KIN CNC 1% 40c	10/17/2003 13:46	4788
OCT03368.SA2_RW_F077	5M Scatt KIN CNC 1% 40c	10/17/2003 13:47	4699
OCT03369.SA2_RW_F078	5M Scatt KIN CNC 1% 40c	10/17/2003 13:48	4869
OCT03370.SA2_RW_F079	5M Scatt KIN CNC 1% 40c	10/17/2003 13:49	4904
OCT03371.SA2_RW_F080	5M Scatt KIN CNC 1% 40c	10/17/2003 13:56	5815
OCT03372.SA2_RW_F081	5M Scatt KIN CNC 1% 40c	10/17/2003 13:59	5947
OCT03373.SA2_RW_F082	5M Scatt KIN CNC 1% 40c	10/17/2003 14:01	6270
OCT03374.SA2_RW_F083	5M Scatt KIN CNC 1% 40c	10/17/2003 14:04	6446
OCT03375.SA2_RW_F084	5M Scatt KIN CNC 1% 40c	10/17/2003 14:07	6695
OCT03376.SA2_RW_F085	5M Scatt KIN CNC 1% 40c	10/17/2003 14:09	7019
OCT03377.SA2_RW_F086	5M Scatt KIN CNC 1% 40c	10/17/2003 14:12	7179
OCT03378.SA2_RW_F087	5M Scatt KIN CNC 1% 40c	10/17/2003 14:14	7604
OCT03379.SA2_RW_F088	5M Scatt KIN CNC 1% 40c	10/17/2003 14:17	7739
OCT03380.SA2_RW_F089	5M Scatt KIN CNC 1% 40c	10/17/2003 14:19	8010
OCT03381.SA2_RW_F090	5M Scatt KIN CNC 1% 40c	10/17/2003 14:22	8400
OCT03382.SA2_RW_F091	5M Scatt KIN CNC 1% 40c	10/17/2003 14:25	8621
OCT03383.SA2_RW_F092	5M Scatt KIN CNC 1% 40c	10/17/2003 14:28	8876
OCT03384.SA2_RW_F093	5M Scatt KIN CNC 1% 40c	10/17/2003 14:29	8852
OCT03385.SA2_RW_F094	5M Scatt KIN CNC 1% 40c	10/17/2003 14:32	9395
OCT03386.SA2_RW_F095	5M Scatt KIN CNC 1% 40c	10/17/2003 14:34	9532
OCT03387.SA2_RW_F096	5M Scatt KIN CNC 1% 40c	10/17/2003 14:37	9772
OCT03388.SA2_RW_F097	5M Scatt KIN CNC 1% 40c	10/17/2003 14:39	9722
OCT03389.SA2_RW_F098	5M Scatt KIN CNC 1% 40c	10/17/2003 14:42	10010
OCT03390.SA2_RW_F099	5M Scatt KIN CNC 1% 40c	10/17/2003 14:44	10355
OCT03391.SA2_RW_F100	5M Scatt KIN CNC 1% 40c	10/17/2003 14:47	10608
OCT03392.SA2_RW_F101	5M Scatt KIN CNC 1% 40c	10/17/2003 15:05	12230
OCT03393.SA2_RW_F102	5M Scatt KIN CNC 1% 40c	10/17/2003 15:06	12291
OCT03394.SA2_RW_F103	5M Scatt KIN CNC 1% 40c	10/17/2003 15:06	12257
OCT03395.SA2_RW_F104	5M Scatt KIN CNC 1% 40c	10/17/2003 15:07	12472
OCT03396.SA2_RW_F105	5M Scatt KIN CNC 1% 40c	10/17/2003 15:19	13503
OCT03397.SA2_RW_F106	5M Scatt KIN CNC 1% 40c	10/17/2003 15:20	13616
OCT03398.SA2_RW_F107	5M Scatt KIN CNC 1% 40c	10/17/2003 15:21	13658
OCT03399.SA2_RW_F108	5M Scatt KIN CNC 1% 40c	10/17/2003 15:22	13556
OCT03400.SA2_RW_F109	5M Scatt KIN CNC 1% 40c	10/17/2003 15:22	13808
OCT03401.SA2_RW_F110	5M Scatt KIN CNC 1% 40c	10/17/2003 15:23	13878
OCT03402.SA2_RW_F111	5M Scatt KIN CNC 1% 40c	10/17/2003 15:24	13873
OCT03403.SA2_RW_F112	5M Scatt KIN CNC 1% 40c	10/17/2003 15:25	13884
OCT03404.SA2_RW_F113	5M Scatt KIN CNC 1% 40c	10/17/2003 15:25	13945
OCT03405.SA2_RW_F114	5M Scatt KIN CNC 1% 40c	10/17/2003 15:42	15254
OCT03406.SA2_RW_F115	5M Scatt KIN CNC 1% 40c	10/17/2003 15:43	14964
OCT03407.SA2_RW_F116	5M Scatt KIN CNC 1% 40c	10/17/2003 15:44	15218

OCT03408.SA2_RW_F117	5M Scatt KIN CNC 1% 40c	10/17/2003 15:45	15258
OCT03409.SA2_RW_F118	5M Scatt KIN CNC 1% 40c	10/17/2003 15:45	15367
OCT03410.SA2_RW_F119	5M Scatt KIN CNC 1% 40c	10/17/2003 15:46	15355
OCT03411.SA2_RW_F120	5M Scatt KIN CNC 1% 40c	10/17/2003 16:07	16983
OCT03412.SA2_RW_F121	5M Scatt KIN CNC 1% 40c	10/17/2003 16:08	16844
OCT03413.SA2_RW_F122	5M Scatt KIN CNC 1% 40c	10/17/2003 16:09	16879
OCT03414.SA2_RW_F123	5M Scatt KIN CNC 1% 40c	10/17/2003 16:10	17047
OCT03415.SA2_RW_F124	5M Scatt KIN CNC 1% 40c	10/17/2003 16:22	17489
OCT03416.SA2_RW_F125	5M Scatt KIN CNC 1% 40c	10/17/2003 16:22	17900
OCT03417.SA2_RW_F126	5M Scatt KIN CNC 1% 40c	10/17/2003 16:23	17839
OCT03418.SA2_RW_F127	5M Scatt KIN CNC 1% 40c	10/17/2003 16:24	17953
OCT03419.SA2_RW_F128	5M Scatt KIN CNC 1% 40c	10/17/2003 16:25	17900
OCT03420.SA2_RW_F129	5M Scatt KIN CNC 1% 40c	10/17/2003 16:26	18042
OCT03421.SA2_RW_F130	5M Scatt KIN CNC 1% 40c	10/17/2003 16:45	19086
OCT03422.SA2_RW_F131	5M Scatt KIN CNC 1% 40c	10/17/2003 16:46	19056
OCT03423.SA2_RW_F132	5M Scatt KIN CNC 1% 40c	10/17/2003 16:47	18885
OCT03424.SA2_RW_F133	5M Scatt KIN CNC 1% 40c	10/17/2003 16:47	18952
OCT03425.SA2_RW_F134	5M Scatt KIN CNC 1% 40c	10/17/2003 16:48	18979
OCT03426.SA2_RW_F135	5M Scatt KIN CNC 1% 40c	10/17/2003 16:49	18995
OCT03427.SA2_RW_F136	5M Scatt KIN CNC 1% 40c	10/17/2003 17:02	19983
OCT03428.SA2_RW_F137	5M Scatt KIN CNC 1% 40c	10/17/2003 17:03	19746
OCT03429.SA2_RW_F138	5M Scatt KIN CNC 1% 40c	10/17/2003 17:04	19814
OCT03430.SA2_RW_F139	5M Scatt KIN CNC 1% 40c	10/17/2003 17:05	19873
OCT03431.SA2_RW_F140	5M Scatt KIN CNC 1% 40c	10/17/2003 17:10	19858
OCT03432.SA2_RW_F141	5M Scatt KIN CNC 1% 40c	10/17/2003 17:10	20276
OCT03433.SA2_RW_F142	5M Scatt KIN CNC 1% 40c	10/17/2003 17:11	20196
OCT03434.SA2_RW_F143	5M Scatt KIN CNC 1% 40c	10/17/2003 17:12	20164
OCT03435.SA2_RW_F144	5M Scatt KIN CNC 1% 40c	10/17/2003 17:13	20152
OCT03436.SA2_RW_F145	5M Scatt KIN CNC 1% 40c	10/17/2003 17:13	19924
OCT03437.SA2_RW_F146	5M Scatt KIN CNC 1% 40c	10/17/2003 17:35	20972
OCT03438.SA2_RW_F147	5M Scatt KIN CNC 1% 40c	10/17/2003 17:36	21573
OCT03439.SA2_RW_F148	5M Scatt KIN CNC 1% 40c	10/17/2003 17:36	21188
OCT03440.SA2_RW_F149	5M Scatt KIN CNC 1% 40c	10/17/2003 17:37	21023
OCT03441.SA2_RW_F150	5M Scatt KIN CNC 1% 40c	10/17/2003 17:38	21171
OCT03442.SA2_RW_F151	5M Scatt KIN CNC 1% 40c	10/17/2003 17:39	21442
OCT03443.SA2_RW_F152	5M Scatt KIN CNC 1% 40c	10/17/2003 17:52	22020
OCT03444.SA2_RW_F153	5M Scatt KIN CNC 1% 40c	10/17/2003 17:52	21505
OCT03445.SA2_RW_F154	5M Scatt KIN CNC 1% 40c	10/17/2003 17:53	21777
OCT03446.SA2_RW_F155	5M Scatt KIN CNC 1% 40c	10/17/2003 17:54	21894
OCT03447.SA2_RW_F156	5M Scatt KIN CNC 1% 40c	10/17/2003 18:16	22363
OCT03448.SA2_RW_F157	5M Scatt KIN CNC 1% 40c	10/17/2003 18:17	22699

OCT03449.SA2_RW_F158	5M Scatt KIN CNC 1% 40c	10/17/2003 18:17	22254
OCT03450.SA2_RW_F159	5M Scatt KIN CNC 1% 40c	10/17/2003 18:18	22874
OCT03451.SA2_RW_F160	5M Scatt KIN CNC 1% 40c	10/17/2003 18:19	22737
OCT03452.SA2_RW_F161	5M Scatt KIN CNC 1% 40c	10/17/2003 18:20	22571
OCT03453.SA2_RW_F162	5M Scatt KIN CNC 1% 40c	10/17/2003 18:24	22919
OCT03454.SA2_RW_F163	5M Scatt KIN CNC 1% 40c	10/17/2003 18:25	22713
OCT03455.SA2_RW_F164	5M Scatt KIN CNC 1% 40c	10/17/2003 18:26	22756
OCT03456.SA2_RW_F165	5M Scatt KIN CNC 1% 40c	10/17/2003 18:27	22995
OCT03457.SA2_RW_F166	5M Scatt KIN CNC 1% 40c	10/17/2003 18:27	22954
OCT03458.SA2_RW_F167	5M Scatt KIN CNC 1% 40c	10/17/2003 18:28	22877
OCT03459.SA2_RW_F168	5M Scatt KIN CNC 1% 40c	10/17/2003 18:29	22785
OCT03460.SA2_RW_F169	5M Scatt KIN CNC 1% 40c	10/17/2003 18:30	22884
OCT03461.SA2_RW_F170	5M Scatt KIN CNC 1% 40c	10/17/2003 18:30	22998
OCT03462.SA2_RW_F171	5M Scatt KIN CNC 1% 40c	10/17/2003 18:31	23105
OCT03463.SA2_RW_F172	5M Scatt KIN CNC 1% 40c	10/17/2003 18:32	23036
OCT03464.SA2_RW_F173	5M Scatt KIN CNC 1% 40c	10/17/2003 18:48	23090
OCT03465.SA2_RW_F174	5M Scatt KIN CNC 1% 40c	10/17/2003 18:49	23297
OCT03466.SA2_RW_F175	5M Scatt KIN CNC 1% 40c	10/17/2003 18:49	23550
OCT03467.SA2_RW_F176	5M Scatt KIN CNC 1% 40c	10/17/2003 18:50	23342
OCT03468.SA2_RW_F177	5M Scatt KIN CNC 1% 40c	10/17/2003 18:51	23367
OCT03469.SA2_RW_F178	5M Scatt KIN CNC 1% 40c	10/17/2003 18:52	23486
OCT03470.SA2_RW_F179	5M Scatt KIN CNC 1% 40c	10/17/2003 18:52	23309
OCT03471.SA2_RW_F180	5M Scatt KIN CNC 1% 40c	10/17/2003 18:53	23429
OCT03472.SA2_RW_F181	5M Scatt KIN CNC 1% 40c	10/17/2003 18:54	23409
OCT03473.SA2_RW_F182	5M Scatt KIN CNC 1% 40c	10/17/2003 18:55	23299
OCT03474.SA2_RW_F183	5M Scatt KIN CNC 1% 40c	10/17/2003 18:55	23478
OCT03475.SA2_RW_F184	5M Scatt KIN CNC 1% 40c	10/17/2003 19:21	24406
OCT03476.SA2_RW_F185	5M Scatt KIN CNC 1% 40c	10/17/2003 19:22	24467
OCT03477.SA2_RW_F186	5M Scatt KIN CNC 1% 40c	10/17/2003 19:22	24279
OCT03478.SA2_RW_F187	5M Scatt KIN CNC 1% 40c	10/17/2003 19:23	24553
OCT03479.SA2_RW_F188	5M Scatt KIN CNC 1% 40c	10/17/2003 19:24	24241
OCT03480.SA2_RW_F189	5M Scatt KIN CNC 1% 40c	10/17/2003 19:25	24277
OCT03481.SA2_RW_F190	5M Scatt KIN CNC 1% 40c	10/17/2003 19:25	24463
OCT03482.SA2_RW_F191	5M Scatt KIN CNC 1% 40c	10/17/2003 19:26	24398
OCT03483.SA2_RW_F192	5M Scatt KIN CNC 1% 40c	10/17/2003 19:27	24284
OCT03484.SA2_RW_F193	5M Scatt KIN CNC 1% 40c	10/17/2003 19:28	24313
OCT03485.SA2_RW_F194	5M Scatt KIN CNC 1% 40c	10/17/2003 19:29	24421
OCT03486.SA2_RW_F195	5M Scatt BANJO CELL EMPTY KINETICS	10/17/2003 19:48	10178
OCT03487.SA2_RW_F196	5M Scatt DODECANE BANJO CELL KINETICS	10/17/2003 20:00	36933

OCT03488.SA2_RW_F197	5M Trans BANJO CELL CNC DODEC 1% 25000CTS	10/17/2003 20:12	102520
OCT03495.SA2_RW_F204	5M Trans CNC 3% DODEC SLOWLY COOLED BANJO	10/17/2003 20:33	99063
OCT03502.SA2_RW_F211	5M Scatt CNC 3% DODEC SLOWLY COOLED BANJO CELL	10/17/2003 20:59	7.79E+06

Supporting Figure 10. Scattering intensity versus Q from data obtained in a 10 s interval after a 1.0 wt% **CNC** in *n*-dodecane-d_{26} sample had remained at 40 °C for 368 s (1), 1824 s (2), 3855 s (3), 10058 s (4), and 33536 s. Note that two oscillations can be detected even with the 10 s collection time in curve (5).

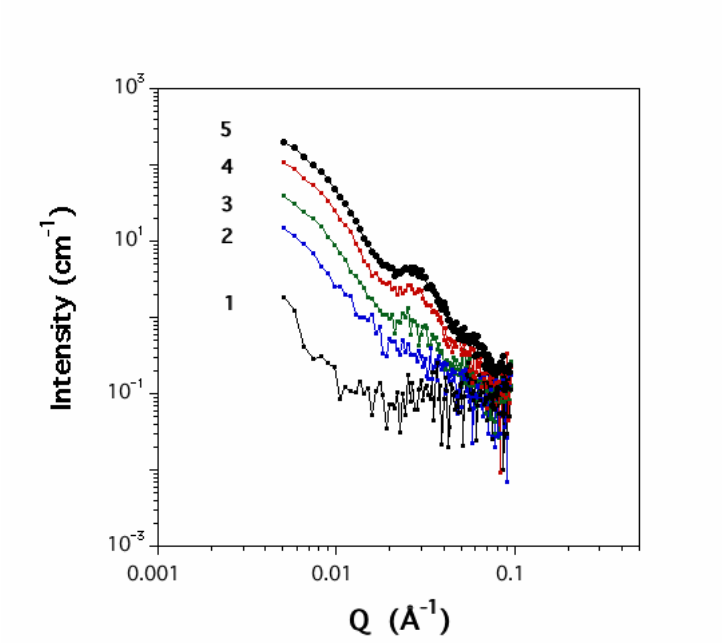

Appendix 1. *Derivation of fractal model equation.*

Our analysis of the fractal nature of our molecular organogels is based upon a kinetic model developed by Dickinson.[7] The conditions under which it should apply to **CNC** and **CeNC** organogels are described in the text.

Then, the average size of aggregates (V_a) can be expressed as in eq. 1, where V_n is average volume of nucleated molecules, V_0 is the volume of a gelator molecule, N_0 is

the concentration of gelator (mol/volume), k is rate constant, $f(t)$ is a time function for Smoluchowski-type aggregation, (i.e., $f(t) = t$ where t is time).

$$V_a = V_n + N_0 \times k \times V_0 \times f(t) \quad (1)$$

When t is sufficiently large, $V_n << N_0 \times k \times V_0 \times f(t)$ and eq. 1 becomes eq. 2.

$$V_a = N_0 \times k \times V_0 \times t \quad (2)$$

The effective volume fraction of aggregates at time t, ϕ_{eff}^t, is proportional to the product of ρ_0 (the density of nucleated molecules, which is determined by gelation temperature, gelator concentration, etc.) and R_a (the average hard-sphere radius of the aggregates) divided by V_a (eq. 3).

$$\phi_{eff}^t \propto \rho_0 \times R_a^3 / V_a \quad (3)$$

In fractal concepts, $R_a \propto V_a^{1/D_f}$, so that eq. 3 can be rewritten as eq. 4.

$$\phi_{eff}^t \propto \rho_0 \times V_a^{(3-D_f)/D_f} \quad (4)$$

Substituting eq. 2 into eq. 4, and changing to a logarithmic form yields eq. 5 the equation we have applied in our analyses.

$$\ln \phi_{eff}^t = C + (3 - D_f)/D_f \ln t \quad (5)$$

---

[1] Lu, L.; Cocker, M.; Bachman, R. E.; Weiss, R. G. *Langmuir* **2000**, *16,* 20-34.

[2] Lu, L.; Cocker, M.; Bachman, R. E.; Weiss, R. G. *Langmuir* **2000**, *16*, 20-34.

[3] Eldridge, J. E.; Ferry, J. D. *J. Phys. Chem.* **1954**, *58*, 992-995.

[4] Khan, S. A.; Royer J. R.; Raghavan, S. R. *Aviation Fuels with Improved Fire Safety: A Proceeding*; National Academy Press: Washington, DC, **1997**, pp 31-46.

[5] a) Almdal, K.; Dyre, J.; Hvidt, S.; Kramer, O. *Polym. Gels Networks* **1993**, *1*, 5-17. b) Khan, S. A.; Royer J. R.; Raghavan, S. R. *Aviation Fuels with Improved Fire Safety: A Proceeding*; National Academy Press: Washington, DC, **1997**, pp 31-46.

[6] Huang, X.; Terech, P.; Raghavan, S. R.; Weiss, R. G. *J. Am. Chem. Soc.*, **2005**, *127*, 4336-4344

[7] Dickinson, E. *J. Chem. Soc., Faraday Trans.*, **1997**, *93*, 111-114.